A study of reactive silica dissolution for determining potential alkali silica reactivity in concrete

Patrick Kao

A report prepared in partial fulfillment of
the requirements for the degree of

Master of Science
Earth and Space Sciences: Applied Geosciences

University of Washington

December 2016

Project mentors:
Juliet Crider
Tom Badger

Internship coordinator:
Juliet Crider

Reading committee:
Juliet Crider
Don Janssen

MESSAGe Technical Report Number: [045]

Executive Summary

Alkali silica reaction (ASR) has been recently identified as an issue relating to problematic performance characteristics of aggregates sourced in western Washington State. An abundance of literature on ASR attributes minerals and rocks containing amorphous silica as initiating the chemical and physical mechanisms that damages concrete. The geological source, composition, and quantity of these reactive aggregates contained in local aggregate resources is unknown. Therefore, an understanding of the structure and properties of amorphous silica in reactive aggregates is essential to the assessment of ASR and consequent expansion in concrete structures.

To better discern this problem, a series of experiments were conducted using two different sources of aggregate (local sand "BH", and a control sand "MT") to observe the behavior of reactive silica in concrete. First, I conducted a point count of grains to determine the composition of each aggregate. Then, under guidance of accelerated mortar bar test ASTM C1260, I mixed 34 mortar bars using 0%, 2%, 4%, 6%, 10%, and 20% chert in the aggregates and measured the resultant expansion. Using the remaining product of alkali solution from the mortar bar tests, I measured the concentrations of NaOH in 10 samples and recorded the consumption of alkali as a result of silica dissolution. I then cut the mortar bars into thin sections and observed reaction within chert grains. From five thin sections, I modeled reaction rate of silica dissolution in chert.

The maximum expansion, or pessimum limit, was recorded at ~0.24% using BH sands containing 2% chert, and at ~0.25% using MT sands containing 10% chert. BH sands, containing 28% volcanic lithics, expanded ~0.20% without added chert. MT sands, containing no volcanic lithics, expanded below deleterious threshold limits, at ~0.032%. From the titration trials, a simple linear regression was inferred between alkali concentration and mortar bar expansion. A maximum of 0.068 moles of alkali was consumed by the highest expansive mortar bar, at ~0.25%. This indicated that remaining free alkali was in excess and therefore, not the limiting reactant in observed maximum expansion limit of mortar bars. Finally, measurements of reaction depth were approximated for 25 chert grains from thin sections of mortar bars containing BH sand and 10% chert. Using values of these measurements, the diffusivity of silica dissolution was found to be between 9.5E-16$\mu m^2/s$ and 8.0E-15$\mu m^2/s$.

I propose that the concentration of NaOH solution from ASTM C1260 tests, and the diffusivity of silica dissolution are applicable in further assessing aggregate susceptibility to ASR. While this project confirms that chert causes ASR in concrete, it was not found in the point count survey of the local aggregate (BH sands). Instead, volcanic lithics that are predominantly andesitic are suspected to be the primary source of reactive aggregates in these sands. It is recommended that similar experiments presented in this report are conducted to determine the reactive properties of volcanic lithics that are used as concrete aggregates.

Table of Contents

1.0 Introduction

Aggregate (typically sand, gravel or crushed rock) is an essential particulate material in construction, comprising three quarters by volume of concrete. It is important to understand the properties of aggregate due to its influence on the durability, thermal and elastic properties in concrete (Godfrey, 1908; Sims and Brown, 1998; Mehta and Monteiro, 2006). Due to the high cost of transportation and large volumes required, it is not economically feasible to ship aggregate long distances. (Alexander and Mindess, 2005). Therefore, it is of fundamental importance to provide a steady, competent supply of quality aggregate sources.

In some cases, aggregate can contain deleterious substances that alter concrete chemistry and cause perpetual durability issues (Mehta and Monteiro, 2006). One such destructive mechanism is a series of chemical reactions called alkali silica reactions (ASR). ASR is first initiated by the dissolution of silica due to attacks by hydroxyl ions (Prezzi et al., 1997), where silicate polymers then bind to alkali ions and forms an expansive gel byproduct (Poole, 2005). The extent of susceptibility to ASR depends upon the degree of atomic disorder and internal surface area within the aggregate grain (Dent Glasser and Kataoka, 1981; Gutteridge, 1985). Chert is conventionally identified as the prevalent reactive aggregate capable of generating ASR. However, minerals and rocks containing other forms of microcrystalline or poorly crystalline hydrous silica have been documented to cause ASR (McConnell et al., 1947; Dent Glasser and Kataoka, 1981).

Availability of a steady supply of high quality aggregates suitable for construction and infrastructure have been of continuing concern in western Washington State, as population growth has fueled demand for construction materials (Shrimer, 2005). However, the region has currently a known aggregate problem, where common aggregate sources are prone to induce ASR. Washington State Department of Transportation (WSDOT) imposes strict standards for aggregate, to mitigate against ASR. However, demand for rapid aggregate source approval limits state testing to accelerated mortar bar tests using ASTM C1260 (WSDOT, 2016). WSDOT has not identified the geological context or mineralogical components of ASR-related problem aggregates in western Washington.

While many have studied aggregate compositions and their effects on initiating ASR (Baingam et al., 2015; Kawamura and Iwahori, 2004; Leemann et al., 2015; Moundoungou et al., 2014; Broekmans, 2004; Ichikawa, 2009; Bektas et al., 2004), very little is known about relationship between silica-mineral microstructure and reaction rate. The key to mitigating the effects of ASR is to understand the mineralogical characteristics of each aggregate and the predictable outcomes from chemical reactions for aggregates with these characteristics. Why does reactive silica cause expansion in concrete and what are the properties that distinguish the forms of reactive silica and their susceptibility to ASR?

This project aimed to estimate alkali silica reaction parameters by running laboratory experiments to induce ASR in concrete with known proportions of chert in aggregate. To do this, I ran a series of mortar bar expansion tests to examine the effects on chert proportion relative to

concrete expansion. I also examined reaction rims around chert grains in concrete thin sections. By measuring the depth at which ASR penetrates the chert grains, I created a model of silica dissolution on as a of a time-based diffusion reaction.

Through this diffusion, it is possible to estimate the reaction rate at which ASR affects chert grains. In principle, the same concepts can be applied to other forms of reactive silica, potentially finding their distinguishing reaction properties. The calculation of reaction rates is a crucial step in understanding the reactivity of silica and macro expansion.

With increasingly stringent standards to protect the longevity of infrastructure, it is important to study the geologic properties of aggregate and screen for problematic components. To meet such standards, one of the objectives of this project is to identify ASR screening methods alternative to the rapid mortar bar test currently adopted by WSDOT.

2.0 Background

ASR are a series of chemical reactions that lead to potential structural weaknesses in concrete (Poole, 2005). Although usually taking place over a few years, ASR is strongly aggressive and can substantially decrease service life of structures (Baingam et al., 2015). These reactions involve alkali hydroxides (usually from alkalis present in cement) and reactive forms of silica within aggregate particles. With the addition of water, the chemical reactions result in an alkali-silica gel product that swells. Depending on reaction temperature, time, and material and proportion type, the accumulation of gel and swelling pressures within concrete may induce and propagate micro fractures (Poole, 2005). This physical expansion and cracking leads to acceleration of deterioration mechanisms, such as freeze-thaw, and ingress of saline water and runoff (Glasser, 1992). Thus, typical deleterious features of ASR could cause fragmental spalling on exposed surfaces, leading to detrimental misalignment of structural elements (Poole, 2005).

ASR expansive potential is complex and poorly understood due to various chemical and physical factors such as quantities of reactants, system porosity, and contact surface area. The microstructure of the cement paste and the grain size distribution of the aggregate is known to influence reactivity and expansion (Glasser, 1992). In addition, certain siliceous materials that occur in natural mineral aggregates react with the alkaline components of cement. Relatively open frameworks associated with particular silica polymorphs exhibit substantially enhanced reactivity towards alkali. Furthermore, pore fluids, regularly dominated by soluble sodium and potassium alkalis, provide a convenient source of hydroxide ions necessary for ASR (Glasser, 1992). Hence, there is considerable interest in correlating measurable chemical and physical parameters with expansive potential.

2.1 Concrete constituents and pore fluid chemistry

Concrete consists of aggregates - a mixture of gravel and sand, in a matrix of cement paste. The water/cement ratio in cement pastes ranges between 0.35-0.55. However, typical cement formulas require a water/cement ratio of only 0.24 for full hydration (Glasser, 1992).

In nature, SiO_2 predominately occurs as the mineral quartz. The framework of quartz is a silicon-oxygen tetrahedron, with four semi-covalent Si-O bonds. Quartz (density 2.65 g/cm3) is the most abundant and stable polymorph characterized by strong bonds requiring high energies to break; hence it is comparatively dense and relatively unreactive, remaining predominantly unaffected by the presence of most strong acids or alkalis (Glasser, 1992). Other frameworks occur within the polymorphs tridymite and cristobalite. These have open, low-density structures and generally occur in rocks with high-temperature origins, such as felsic volcanic rocks (Heaney et al., 1993). Tridymite (density 2.26 g/cm3) has sheets in hexagonal rings that lie directly over one another, creating continuous tunnels normal to the sheets. In cristobalite (density 2.32 g/cm3), the structure involves three sheets of hexagonal rings that do not superimpose (Huang et al., 2012). Because their frameworks are more open relative to the denser, more tightly bonded quartz, both tridymite and cristobalite are more susceptible to alkali reactivity (Glasser, 1992).

Disordered or randomly oriented silica frameworks also exist, and are often present within aggregate sources. Depending on their physical forms and mode of geological origin, they have a variety of generic names, including opal, chert, and chalcedony (Glasser, 1992). Chert can be defined as a siliceous rock consisting predominantly of cryptocrystalline non-clastic silica and occurring as beds, nodular masses or veins in sedimentary rocks (Smith, 1960). Chert's thermodynamic metastability and comparatively open structures makes it susceptible to alkali reactivity (Glasser, 1992).

Volcanic lithic fragments have been previously documented to cause ASR (Shrimer, 2005; Ichikawa and Miura, 2007; Katawaki et al., 1989; Kobayashi et al., 1989; Ichikawa, 2009). This is primarily due to the framework of silica found in volcanic glass and intermediate and felsic volcanic lithic fragments containing significant glassy matrices, behaving as weak to moderate reactive silica particles in concrete. X-ray diffraction patterns of andesitic grains have also indicated both the presence of cristobalite and tridymite silica polymorphs. In Washington State, mass spectrometry and x-ray florescence analyses of andesite samples from Mt. Adams confirms a 50%-62% silica composition within the matrix (Dunn and Sen, 1994), consistent with the compositional definition for andesite. In Japan, andesite samples containing volcanic glass up to 36% was responsible to cause at least one instance of a structural failure (Kawamura et al., 1989).

Significant work has been done on water-silica interactions. Using Born-Oppenheimer local spin density molecular dynamics (BO-LSD-MD), Cheng et. al. (2002) studied size dependence and interactions between singular SiO_2 molecules and H_2O clusters (one to six). Stability of the silica molecule was destroyed as more water molecules were added to the interaction, leading to the breakdown of two Si=O double bonds and the formation of four Si-OH (silanol) single bonds. With

open structures (such as on amorphous silica), higher reactive sites exist, correlating to higher bond weakening and breaking of SiO_2 (Young, 1958). This is the concept of dislocation density, or structural defects within the crystal lattice that result in the prevalent occurrence of unsatisfied charges of non-bridging oxygen. The degree of dislocation is important in determining the solubility of silica, as defect-free crystal lattices are less prone to attack by dissolution in a high pH environment (Figure 1) (Dent Glasser and Kataoka, 1981; Broekmans, 2002). Wenk et al. (2008) showed that dislocation density of quartz increases with increased deformation within granitic and mylontic rocks; this increase in dislocation density correlated with increased ASR related expansion when the quartz was tested as aggregate in mortar bars.

The porosity within cement allows the migration of water and dissolved cations to reach amorphous silica. The pore fluid in concrete is an alkaline solution that is typically comprised of Na^+, K^+, Ca^{2+}, OH^-, and $SO4^{2-}$ ions (Glasser, 1992). The cement paste in concrete contains interconnected microscopic pores through which the excess water with ions in solution can migrate (Farny and Kerkhoff, 2007). This direct contact of pore fluid, cement hydration products, and aggregate particles allows for a series of reactions to commence by mass transport of OH^- and alkali ions (Glasser, 1992).

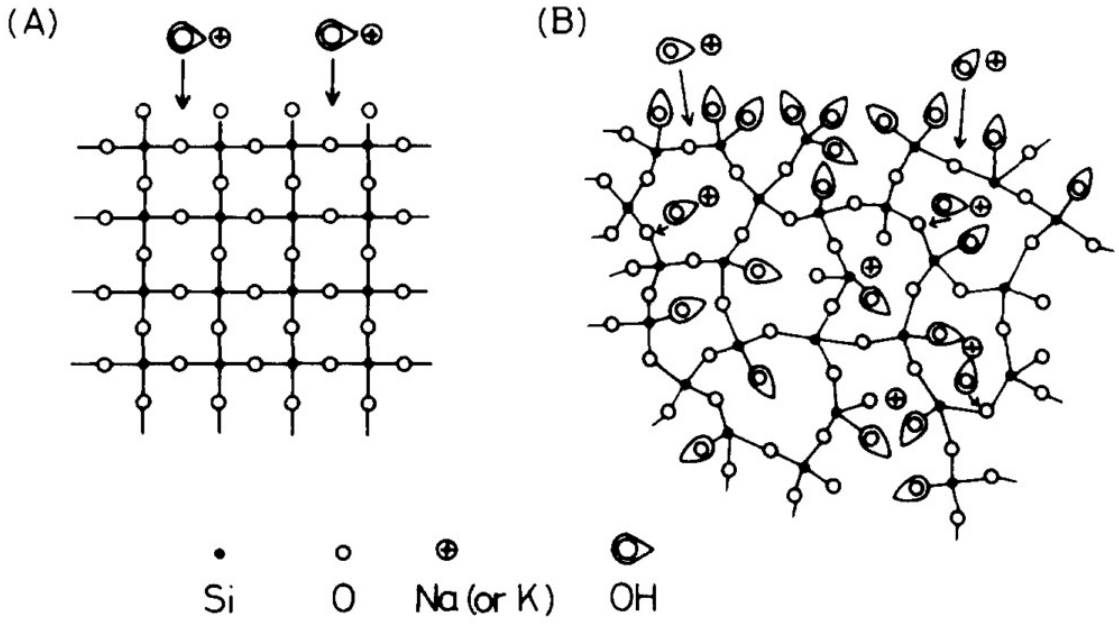

Figure 1. Attack of alkali on well crystallized silica (A) and poorly crystallized silica (B), from (Dent Glasser and Kataoka, 1981)

2.2 Transport of OH^- and alkali ions

Normally, in the presence of water, unsatisfied charges at the silica surface and in the interstitial sites are neutralized by OH- and H+ ions (Carman, 1940; Prezzi et al., 1997). This depolymerization of silica by hydration can be expressed as the reaction:

$$\equiv(Si - O - Si\text{-})_s + H_2O_{aq} \rightarrow 2 \equiv (Si - OH)_s \qquad \text{(eq. 1)}$$

Silica surfaces are left with a weakly acidic character when hydrogen ions are freed because the bonding in silica (Si – O – Si) is stronger than the bond in hydroxyl (O-H) (Carman, 1940). Hydroxl ions progressively attack the ≡(Si – O –) bonds, resulting in network dissolution of silica (Rajabipour et al. 2015):

$$\equiv(Si - OH)_s + 3(OH^-)_{aq} \leftrightarrow (Si(OH)_4)_{aq} \qquad \text{(eq. 2)}$$

In the depolymerization process, all four bonds in a tetrahedron may react, thereby forming silicate ions and polymers, such as the monomer $Si(OH)_4$ (Prezzi et al., 1997).

Silica is more soluble at extreme values in strongly alkaline environments than it is at neutral values (Alexander et al., 1954). At the high pH characteristic of alkali solutions, the silica surface is negatively charged and attracts cations from solution. The sequence of reactions involved in silica depolymerization, proceeding from pH 9 to pH > 12, is as follows (Heaney et al., 1993; Broekmans, 2004; Fernandes, 2005):

$$(Si(OH)_4)_{aq} \leftrightarrow (H_3SiO_4^-)_{aq} + H^+ \text{ at pH} > 9 \qquad \text{(eq. 3)}$$

$$(H_3SiO_4^-)_{aq} \leftrightarrow (H_2SiO_4^{2-})_{aq} + H^+ \text{ at pH} >10 \qquad \text{(eq. 4)}$$

$$(H_2SiO_4^{2-})_{aq} \leftrightarrow (HSiO_4^{3-})_{aq} + H^+ \text{ at pH} > 11 \qquad \text{(eq. 5)}$$

$$(HSiO_4^{3-})_{aq} \leftrightarrow (SiO_4^{4-})_{aq} + H^+ \text{ at pH} >12 \qquad \text{(eq. 6)}$$

The solubility of well crystallized silica is negligible at high pH, occurring only at the surface of the aggregate; conversely, solubility of disordered silica increases exponentially with pH (Mukhopadhyay et al., 2009). This is due to the high hydroxyl concentration and the high pH values that triggers the chemical reaction with reactive silica components. High concentration of alkali ions contributes to an equally high concentration of hydroxyl, maintaining equilibrium in the pore solution (Ramos, 2013).

However, in an alkaline medium where NaOH is present, the H+ ions are replaced by Na+ cations that cannot form strong bonds with the oxygen ion (unlike H+) and are more easily hydrated. As a result, Na+ ions are readily ionized and a colloidal suspension is formed with silica particles (Prezzi et al., 1997).

If there is still an excess of NaOH after the hydroxyl groups at the surface of silica have been neutralized, then the internal –Si – O – Si- links can be disrupted. In alkaline solutions, silica is much more easily dissolved, with hydroxyl ions being the catalyst (Iler, 1979). These hydroxyl ions

are chemisorbed onto the silica surface, increasing the coordination number of the silicon ion to more than four, thus weakening the oxygen ion bonds to the underlying silicon ions. Because of the open structure of amorphous silica, there are sites on the surface between oxygen ions large enough to accommodate additional hydroxyl ions. As a result of the adsorption of hydroxyl ions on the surface and the increase in the coordination number of silicon, Si-O bonds become unstable and silicate ions go into solution. This process increases the negative charge on the surface, and silica is constantly exchanged in an attempt to reach equilibrium with the aqueous solution (Prezzi et al., 1997).

2.3 The properties of alkali-silica gel

The breakdown of silica surfaces and the interaction between silicate polymers and alkali ions produce a viscous alkali-silica gel that swells upon water absorption. As the gel absorbs moisture, it increases in volume and generates pressures sufficient to disrupt the fabric of the concrete (Poole, 2005). While the gel is often formed at the aggregate-cement paste interfaces, swelling within the aggregate particles may occur (Dent Glasser and Kataoka, 1981).

The stoichiometric composition of alkali silica gel is still not fully understood (Ramos, 2013). Scanning electron microscope (SEM) with energy dispersive spectrometry (EDS) and X-ray diffraction (XRD) have been used in attempts to define ASR gel composition and understand reaction kinetics (Thaulow et al., 1996; Kawamura, 1998; Diamond, 2000; Kawamura and Iwahori, 2004; Peterson et al., 2006; Fernandes et al., 2004, 2007; Fernandes, 2009; Šachlová et al., 2010; Katayama, 2012; Locati et al., 2012). Helmuth and Stark (1992) suggested that ASR gels are two-component mixtures of alkali-calcium-silicate-hydrate (C-N-(K)-S-H) gel (considered as C-S-H), and alkali-silicate hydrate (N-(K)-S-H gel) (or A-S-H) of nearly fixed compositions (Helmuth and Stark, 1992). Wieker et al. (1998, 2000) proposed that the structure of ASR gel is similar to that of kanemite ($Na_2O_4(OH)_2\ H_2O$). In addition, Peterson et al. (2006) reported that the crystallization of the gel over time has been observed and related to okenite ($CaSi_2O_5\ 2H2O$) with potassium and sodium substitutions. The current consensus is that the composition and amount of the cement (and admixtures), water, and ingress of foreign ions directly influences the chemical composition and expansion ability of the gel (Prezzi et al., 1997).

Alkali-silica gel usually exhibits an amorphous structure under X-rays and is optically isotropic, with only a modest birefringence (St John et al., 1998). The gel also exhibits a wide range of viscosities depending on the amount of incorporated water, although the relations between composition, viscosity, and swelling are not fully understood (Haha, 2006). Davis and Oberholster (1986) used geometrical expressions, such as massive, sponge-like, rod-like, blade-like, and rosette-like, to describe the morphology of the observed gel products in ASR-related studies. The reactivity is a function of surface area, crystallinity, and hydration state. In more porous aggregates, such as cherts, the true surface exposed to attack is much greater than the apparent geometric surface area (Glasser, 1992).

3.0 Scope of work

The project objective was to test ASR response of two different aggregates with additional chert by observing the conditions of these aggregates in concrete samples in a series of laboratory controlled experiments. By immersing these concrete samples in heated sodium hydroxide solution to induce ASR, the project was intended to: 1. observe the deleterious effects of chert with ASR related swelling pressures, and 2. predict depolymerization rates of silica in chert grains. A flow chart is provided in Appendix B (Figure B-1).

I collected data through a 10-month period, running 34 trials of an accelerated mortar bar expansion test (method ASTM C1260). I then cut 34 concrete samples and mounted them onto thin sections, where I examined ASR affected surfaces using a petrographic microscope. Furthermore, I measured reaction rims depths from chert grains affected by ASR using a polarized light microscope (PLM). Finally, I developed a diffusion script to model and predict reaction rate of dissolution in chert.

These experiments were conducted in laboratory facilities at the University of Washington. Samples of aggregate were provided by Cowden Gravel & Ready Mix, Inc. and LafargeHolcim. Keokuk chert samples were obtained from Neolithic Flintknapping Supplies.

4.0 Methods

I ran a series of laboratory experiments to evaluate the influence of varying proportions of chert on ASR-related expansion in concrete. The experiments follow a standard protocol (ASTM C1260). I ran experiments with two different aggregates, the Cowden Alm Pit (“BH”) and LaFarge St Gabriel de Brandon (“MT”) sands (described below).

4.1 Selection and description of aggregate

Different aggregate sources show different susceptibility to ASR when used in concrete. I studied sands from two different sources and added chert from a third source to increase the proportion of reactive silica in experiments on ASR. Initially, I examined the sand samples under thin sections and conducted a 50-point count of each source (Section 5.1), noting their grain composition.

4.1.1 Alm Pit, Bellingham area, Washington

The Alm Pit, owned and operated by Cowden Inc., is located within the Nooksack River valley, in the western portion of the North Cascades and approximately 15 miles northeast of Bellingham. It is the source of the BH aggregate. This aggregate was selected for investigating ASR expansive potentials by recommendation and selected due to its location in Western Washington. The aggregate sample from the Alm Pit is a dark greyish, sub-rounded to sub-angular sand and gravel.

Sand at the Alm pit is likely either glacial outwash or fluvial in origin, with provenance at Mount Baker volcano, the North Cascades foothills and crystalline core, or the Coast Plutonic Complex (British Columbia). Lapen (2000) divided regional units into three categories: pre-Tertiary rocks,

Tertiary rocks, and Quaternary deposits. The pre-Tertiary rocks consist of oceanic lithologic packages of varying age, structure, and metamorphic history (Misch, 1966; Brown, 1987). Tertiary rocks are extensive in the area and consist of the Chuckanut and Huntingdon Formations, which are primarly beds of shales, siltstones, sandstones, clay, conglomerates, and coal (Daly, 1912; Johnson, 1982, 1984). Quaternary deposits in the Whatcom basin and Skagit River area are mainly material derived from the four stades of the late Wisconsinan Fraser Glaciation. Tills from these glacial deposits are generally dense, unstratified diamicts of gravel and sand with silt and clay and interspersed boulders and cobbles. The glacial outwash is generally loose, well sorted cobbly gravels, sandy gravels, gravelly sands, sands and silts (Dragovich et al., 1997).

In the post-glacial Nooksack River valleys, modern streams reworked Fraser-aged glacial deposits. This Nooksack River alluvium has been characterized as well stratified and sorted deposits composed of rounded cobbly gravel, gravel, sandy gravel, gravelly sand, silt, clay, and peat. The alluvium was noted to be predominately andesitic in composition (Easterbrook, 1962; Kovanen and Easterbrook, 2001; Cameron, 1989).

4.1.2 Saint Gabriel Pit, Quebec

The MT aggregate is from the Saint Gabriel Pit, owned and operated by LafargeHolcim, is located within the St. Lawrence lowland, approximately 50 miles north of Montreal. This aggregate was chosen as a non-reactive control, as recommended by Dr. Robert Shogren at LafargeHolcim. The aggregate sample from the Saint Gabriel Pit is a rusty brown, sub-rounded to sub-angular sand and gravel.

Sand at the Saint Gabriel pit includes quartz, plagioclase, microcline, pyroxenes, hematite, sandstones and lithics of plutonic origin. The bedrock under the Montreal area and part of the St. Lawrence Platform consists of Paleozoic aged limestone, calcareous shale, sandstone and dolostone. These units represent a slightly deformed shelf of a larger Cambrian-Ordovician assemblage of sedimentary rocks (Prest and Keyser, 1977).

Stretching between 20 west and 120 miles east of Montreal sits the Monteregian Hills. These Mesozoic aged features consist of alkaline igneous intrusions, among which nepheline-bearing diorites and syenite, gabbros, pyroxenites, and granites exist (Eby, 1984; Barkov and Martin, 2016). Surficial deposits of the region consist of layered glacial and interglacial sediments formed in the last 70,000 years during the Wisconsin advances. Deposits from the Malone and Fort Covington advances vary from clayey silty till to silty sandy tills (Prest and Hode-Keyser, 1975). Interglacial and younger sediments include lacustrine silts, marine, estuarine, and alluvial sediments, and peat (Boyer et al., 1985). It is likely that the MT sands are derived from glacial deposits sourced in the Monteregian Hills.

4.1.3 Keokuk Chert, Osage Series

Chert is an ambiguous and general term associated with siliceous sedimentary rocks. Often occurring as bedded deposits associated with deep-water sediments, they also form nodules in shallow-water limestones as a product of diagenesis (Boggs, 1992). I selected the Keokuk Chert as a reactive silica for the mortar bar experiments.

The Keokuk formation of the Osage series is a Mississippian aged carbonate stratum, cropping out in abundance from Illinois in the north to Oklahoma in the south. Part of the Osage Series, the Keokuk formation is composed primarily of cherty limestone and dolostone with minor shale beds (Owen et al., 1852). In southeastern Iowa, the Keokuk contains crinoidal chert with abundant specular fossil fragments (Smith and Gilmour, 1979).

A study of Keokuk chert sourced from Pike County in Illinois used X-ray fluorescene to analyze samples for their major oxide composition (Table 1) (James and Hester, 1974).

Table 1 Oxide composition of Keokuk chert (James and Hester, 1974)

	SiO_2	Al_2O_3	Fe_2O_3	MnO	CaO	CO_2
Keokuk chert sample	96.6	0.13	0.13	0.022	1.68	1.28

Spalls of the Keokuk chert were obtained from Neolithic Flintknapping Supplies, quarried in northeastern Oklahoma. The chert is white to beige in color and partially coated with an iron oxide veneer. Under thin section, the chert consists of micro-silica grains of less than 20 microns in size.

Crushed chert fragments were typically very angular, consistent with breaking in conchoidal fractures. Therefore, the chert was crushed, then partially rounded using silicon carbide grit within a rock tumbler for a period of 4 days. The chert was then sieved to the same grain size range as the other aggregate used for the experiments.

4.1.4 Type I-II Portland Cement

ASTM C1260 evaluates the reactivity of specific cement-aggregate combinations. So while the sieve size of aggregates and proportions within the concrete is standardized, a range of acceptable cements can be used to make the concrete for the expansion test, as specified in ASTM C150 (2016). All mortar bar tests in this project used a type I-II cement. The chemical composition of this cement and the specification limit is given in Table 2 as follows:

Table 2 Chemical Analysis of type I-II cement (LafargeHolcim, 2016)		
Item	**Spec limit**	**Result (% composition)**
SiO_2	-	20.1
Al_2O_3	6.0 max	4.7
Fe_2O_3	6.0 max	3.4
CaO	-	64.0
MgO	6.0 max	0.9
SO_3	3.0 max*	3.1
CO_2	-	1.9
Limestone	5.0 max	4.3
$CaCO_3$ in Limestone	70 min	98
ASTM C150-09 and AASHTO M85-09 Optional Chemical Requirements		
Na Equivalent	0.60 max	0.55
* May exceed 3.0% SO3 maximum based on ASTM C1038 (hydraulic expansion) results of <0.02% expansion at 14 days.		

4.2 Mortar bar experiments using modified ASTM C1260

Since concrete deterioration due to ASR takes place over a span of years, accelerated mortar bar tests are commonly used for evaluating ASR reactivity of aggregate. ASTM C1260 (or AASHTO T 303) has been widely adopted for assessing potential reactivity of aggregate, because it prescribes a convenient two-week testing period. This rapid test method involves measuring the length change of mortar bars before and after the samples are stored in a strongly alkaline solution at an elevated temperature (ASTM, 2014).

Following ASTM C1260, aggregates were sieved to between 4.75 mm and 150 µm, as indicated in Table 3 below. I mixed aggregates with cement and water using a mechanical concrete mixture for a period of four minutes. I then proportioned the materials using 1 part cement to 2.25 parts graded aggregate, with a cement to water ratio equal to 0.47 by mass. For each aggregate, I ran mortar bar trials with fixed amounts of additional chert in the sand: 0%, 2%, 4%, 6%, 10% and 20%. Each trial (aggregate type and chert percent) was run in triplicate. A full list of mortar bar samples and associated chert content is given in Appendix A (Table A-1).

Mortar molds measuring 25mm x 25 mm x 255mm (Appendix B, Figure B-2) were filled with the concrete mixture and left at room temperature and covered with a moist cloth for 24 +/- 2 hours. The specimens were then removed from molds and placed into a sealed container in a water bath at 80+/- 2.0 C for a period of 24 hours.

Table 3. Size distribution of aggregate clasts		
Sieve Size		
Passing	**Retained on**	**Mass %**
4.75mm (No. 4)	2.36 mm (No. 8)	10
2.36 mm (No. 8)	1.18 mm (No. 16)	25
1.18 mm (No. 16)	600 µm (No. 30)	25
600 µm (No. 30)	300 µm (No. 50)	25
300 µm (No. 50)	150 µm (No. 100)	15

Initial measurements were taken using a length-change dial comparator accurate within 0.0001 inches (Appendix B, Figure B-3). After the initial reading, the mortar specimens were placed in sealed containers with one liter of 1 M NaOH solution for full submersion. The containers were placed in an oven at 80+/- 2.0 C and kept in submersion for a period of 14 days (Appendix B, Figure B-4). Subsequent comparator measurements were carried out daily, at 24 +/-2 hour intervals. The difference between the initial comparatory reading of each sample and the reading at each period to the nearest 0.001% were recorded as an indication of sample expansion. Total expansion observed in each of the three trials was averaged; experimental error was calculated as the standard deviation from the three trials.

An optional appendix to the C1260 standard classifies expansion of 0.10% or less at 14 days as innocuous behavior. Expansions of more than 0.20% are indicative of potentially deleterious expansion. Between 0.10% and 0.20%, aggregates are considered to exhibit either innocuous or deleterious behavior in field performance (ASTM, 2014). Detailed experimental procedure for this ASTM C1260 is found in Appendix C (Procedure C-1).

ASTM C1260 did not specify a quantity of NaOH per test. For the proposes of this project, the ASTM C1260 test has been modified to standardize the amount of NaOH solution per sample to one liter.

4.3 Thin section analysis

Mortar bar specimens were removed from the 1 liter 1M NaOH solution after 14 day tests and allowed to dry in room temperature. In preparation for petrographic thin sections, each mortar bar was split and cut into approximately 35 x 25mm x 12mm blocks using a mechanical saw. Surfaces of these blocks were smoothed and polished (Appendix B, Photo B-5). Each block was then examined and selected for thin section mounting based on the prevalence of chert grains along the plane of interest. Selected blocks were placed on individual glass microscope slides with epoxy, and reduced to a thickness of approximately 20 µm (0.0008 in.).

Petrographic examinations of concrete samples were carried out via polarized light microscopy (PLM) (Olympus model BX-41) on thin sections impregnated with UV-active fluorescent dye. UV illumination visually indicated fractures caused by ASR.

BH mortar bars containing 10 percent chert were cut and prepared into five thin sections, and reaction rims observed as ASR within chert grains were measured. These reaction rims were identified in cross and plane polarized light as darkened discolored sections within chert grains exhibiting deterioration and a diffusive-like reaction front. Reaction rims were measured between the aggregate-cement contact surface and within the aggregate grain (Figure 2) using a stage micrometer and a microscope reticle.

The process of making thin sections does not consider the geometry in which the grains were cut. Therefore, reaction rims had the potential of appearing distorted, exaggerating the physical extent of reaction. Due to this distortion, the minimum penetration distance of reaction rims into the grains was recorded.

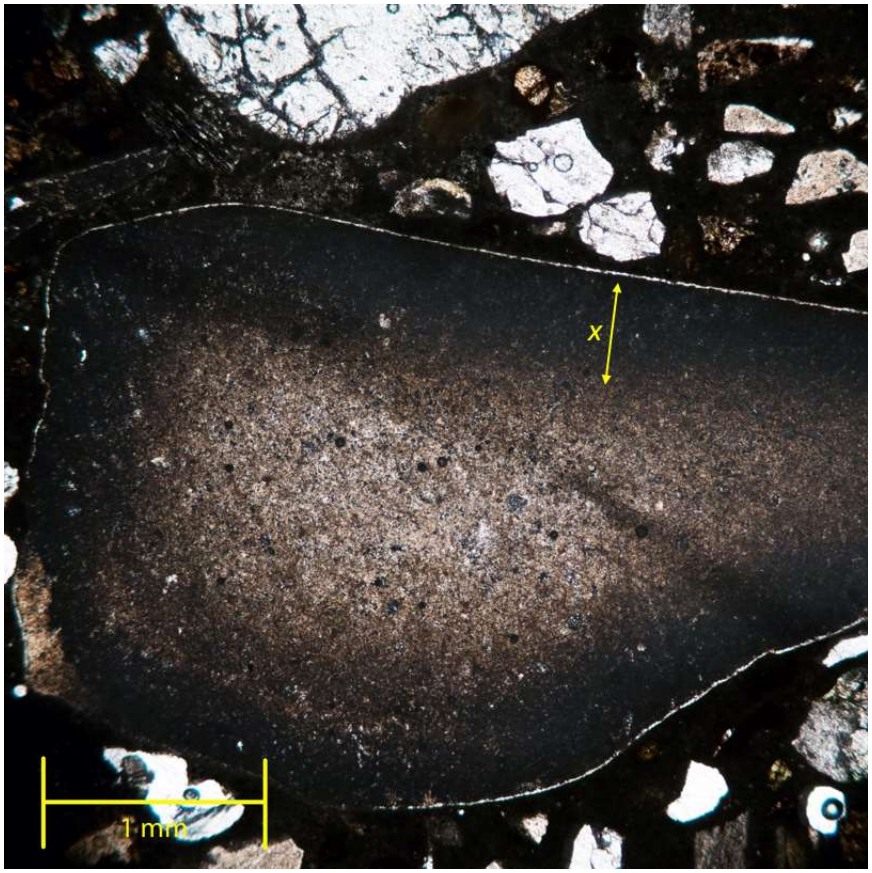

Figure 2. Reaction rim developed around a chert grain, as photographed in plane polarized light. Note the enervation of observed reaction towards the center of the grain. *X*, as indicated in this figure shows the approximate distance used as reaction depth.

4.4 SEM analysis of Keokuk chert

Complementary to the petrographic examination, a scanning electron microscope (SEM) (JEOL model JSM- 6010PLUS/LA) was used for high magnification inspection of a bare rock chert grain that was not subjected to ASTM C1260 (Figure 7). SEM imaging provided a view of the surface texture of chert, and helped in understanding chert-alkali interactions. The grain, measuring

20mm in length and 8mm in height, was gold coated and observed using secondary election imaging between 10,000 and 20,000x magnification. Due to the limitation in space of the SEM analysis stage, back scattered imaging and x-ray microanalysis of thin sections and chert reaction rims were not conducted.

4.5 Modeling experiment results for silica dissolution

A time dependent Fick's diffusion equation (Fick, 1855) was adapted to express the diffusion of ASR in chert grains. This equation is given as Eq. 1, where *y* expresses the initial concentration of alkali, and *x* is the penetration of alkali into the grain over time, *t*. *Cs* is the concentration of alkali at the cement-grain interface, *Co* is concentration at the end depth at time *t*. *D*, diffusion coefficient, and *rs*, reactive silica consumption are unknowns.

$$y = ((Co - Cs)\left(\mathrm{erf}\left(\frac{x}{2\sqrt{Dt}}\right) + Cs\right) - rs \qquad \text{Eq. 1}$$

A range of reaction rims widths of ASR-affected chert grains from an individual sample (ex. BH-10) were used as approximate values of penetration depth (*x)* at the termination of the ASTM C1260 test (14 days).

Variable *rs* is the alkali concentration loss due to various factors affecting the availability of hydroxyl ions in the system. These factors include: consumption by other reactive silica in aggregate, NaOH concentration consumption during the ASTM C1260 test, the percent of chert grains incorporated into aggregate, cement mixture chemistry, and temperature of NaOH solution in contact with aggregate.

The end of the experiment integrates all these variables. For six samples (MT-0, 2, 4, 6, 10, and 20), I measured the concentration of NaOH solution after 14 days as an approximation for *rs*. To do this, I titrated the solutions using acetic acid and a phenolphthalein indicator. Procedures are provided in Appendix A. I calculated *rs* by using the concentration loss of alkali at a given expansive value (Figure 6). This can be expressed as:

$$rs_{\mathrm{m}} = 1 - M = -0.1405x_{\mathrm{e}} + 0.9758 \qquad \text{Eq. 2}$$

Where rs_m is the molar concentration of reactive consumption, *M* is the molar concentration of alkali solution, and x_e is the percent expansion of mortar specimen. Note that *rs* is solved by converting rs_m from molar concentration to g/μm^3.

Known variables in Eq.1 are used to solve for diffusivity via a MatLab script (Appendix C, Figure D-1).

5.0 Results

This section presents expansion test results, hydroxyl concentration measurements, and chert grain reaction rim measurements. The information obtained from the experiments are used as parameters for the model.

5.1 Aggregate composition

I determined the percent composition of the aggregates by measuring the intermediate axis of each grain and dividing the identified mineral/rock by the approximate volume of total measured grains. BH aggregate used in the experiments was a mixture of primarily fine grained feldspathic and quartzitic sedimentary lithics and intermediate volcanic lithics. MT aggregate was a mixture of mafic and intermediate silicate minerals and plutonic lithics. Gabbro, diorite, and granodiorite accounted for over half the composition. Microcline, quartz, plagioclase, and sandstones were also identified. Table 4 lists the lithologic constituents of the BH and MT aggregate.

Table 4: aggregate composition of aggregates	
BH sands	
Lithology	Percent of aggregate composition
Individual quartz grains	8.6
Individual feldspars grains	15.2
Quartz or feldspathic sandstone	13.4
Shale and siltstone	23.2
Lithic sandstone	3.2
Volcanic lithics (andesite)	28
Kyanite	0.5
MT sands	
Lithology	Percent of aggregate composition
Quartz	11.5
Plagioclase	3.9
Microcline	5.4
Pyroxene	1.6
Hematite	3.8
Arkosic sandstone	6.1
Lithic sandstone	2.0
Gabbro	26
Diorite	13.5
Granodiorite	13.3
Granite	7.8
Nepheline syenite	1.8
Aplite	1.8
Hornfels	1.5

5.2 Concrete expansion with known proportions of chert

Per ASTM C1260 guidelines, the two aggregates of unknown reactivity were mixed into mortar bar samples and subjected were subjected to the 1M NaOH solution at 80°C. Thirty-six mortar bars were prepared: three trials of six different chert proportions for two different aggregate sources. Of the 36 mortar bars prepared, two fractured during extraction from molds. Thus, the remaining thirty-four mortar bars represented 0, 2, 4, 6, 10, and 20% proportioned chert in each of two aggregate sources. These bars were measured daily for 14 days. A summary of all trials is presented in Figures. 3a and 3b.

For all trials, between days two to four of the experiments, a gel-like substance began forming on the mortar bar specimens. This transparent substance appeared to be a homogeneous byproduct of a solution-concrete reaction, forming as spotted textures across the surface of the concrete. No chemical analysis of the gel was performed. There was no visual loss in concrete due to the formation of the gel, and the gel did not hinder obtaining expansion measurements.

For trials with BH aggregate, the greatest expansion was observed in mortar bars containing 2% added chert, with an average expansion of 0.24% +/- 6.8E-3%. Total expansion decreased with greater proportion of additional chert (Figure 4). Trials with four and six percent chert expanded 0.17% +/- 1.0E-2% and 0.18% +/- 7.6E-3% respectively, compared to 0.20% +/- 1.5E-2% for no added chert. BH trials with 10% and 20% added chert expanded less than the ASTM “innocuous behavior” criteria, at 0.098% +/- 5E-4% and 0.64% +/- 1.7E-3%.

For trials with MT aggregate, the greatest expansion was observed in mortar bars containing 10% added chert, with an average expansion of 0.25% +/- 3.3E-3%. Total expansion decreased at 20%, to 0.22% +/- 1.2E-3%. Trials with four and six percent chert expanded at 0.23% +/- 1.5E-2% and 0.23%+/- 0% respectively. The control aggregate with no added chert and 2% added chert expanded less than the ASTM “innocuous behavior criteria”, at 0.032%+/- 3.9% and 0.127%+/- 7.7E-3% respectively.

In both sets of trials, the maximum expansion of the BH and MT mortar bars was observed between 0.24% and 0.25% expansion. For trials MT-4 through MT-20, expansion exceeded the ASTM deleterious threshold of 0.2%. In contrast, for trails BH-0 and BH-2, expansion exceeded this threshold criteria, and decreased rapidly with increasing amount of chert. MT control specimens yielded the lowest expansion of any mortar samples, below 0.05%, while the BH control specimens were near or at 0.2%.

Daily length change per specimen are provided in Appendix D, (Table D-1 and D-2).

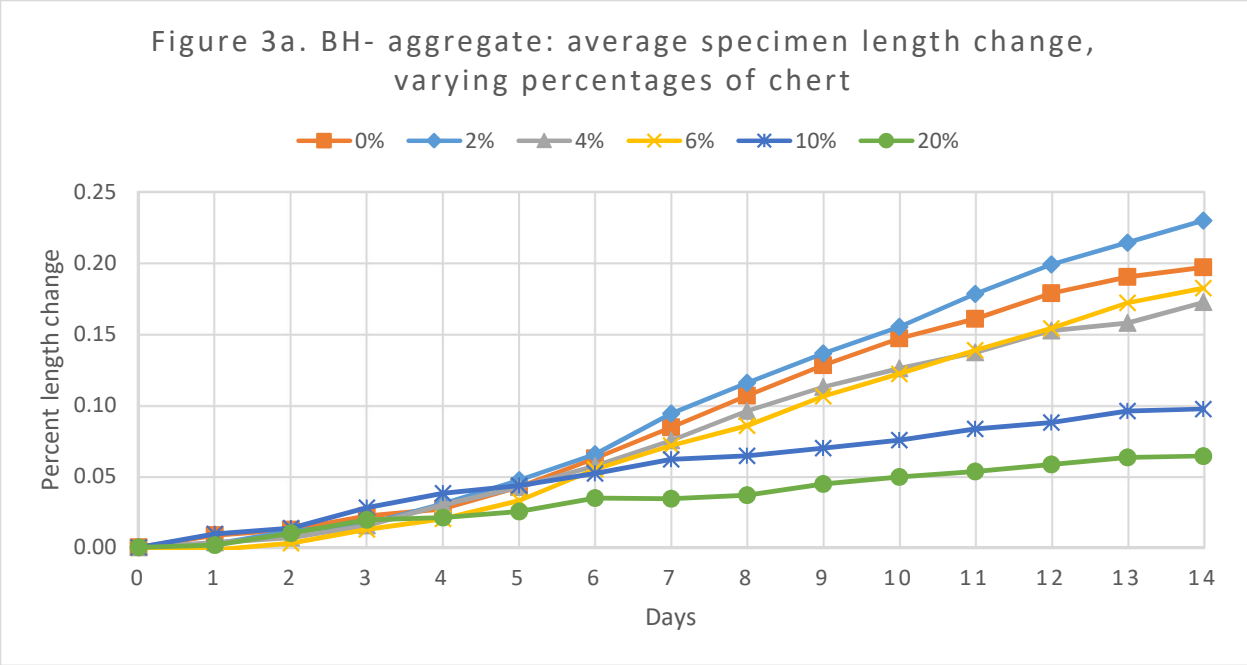

Figure 3a. Summary of BH accelerated mortar bar tests.

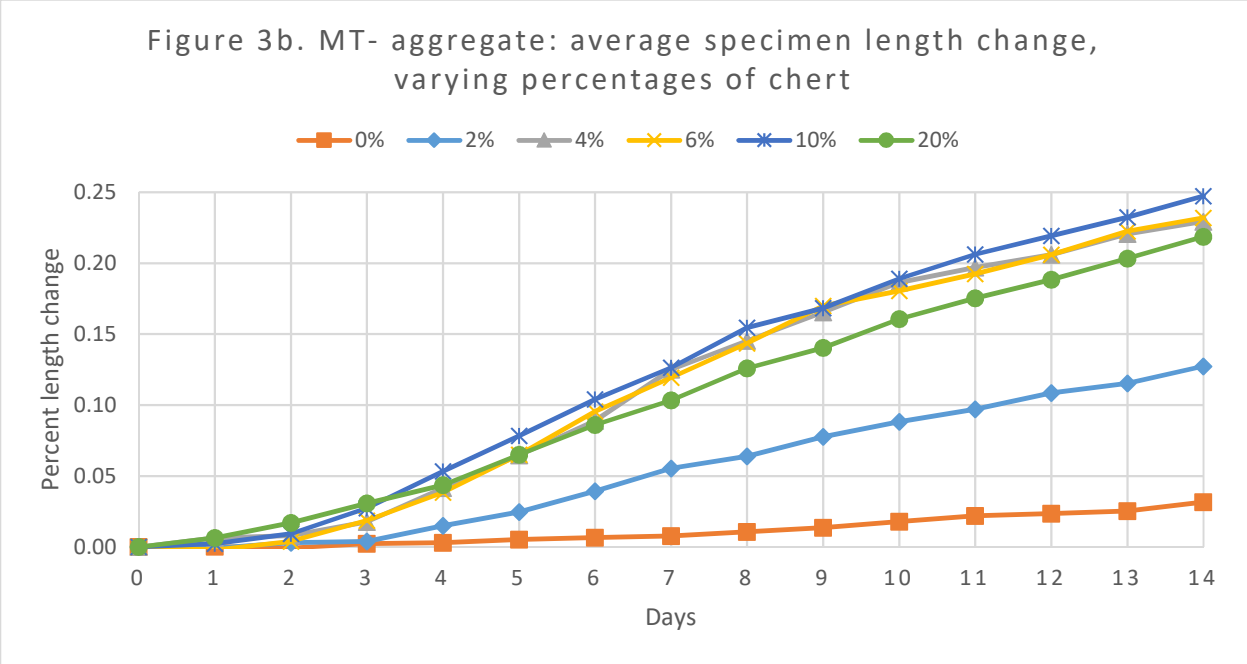

Figure 3b. Summary of MT accelerated mortar bar tests.

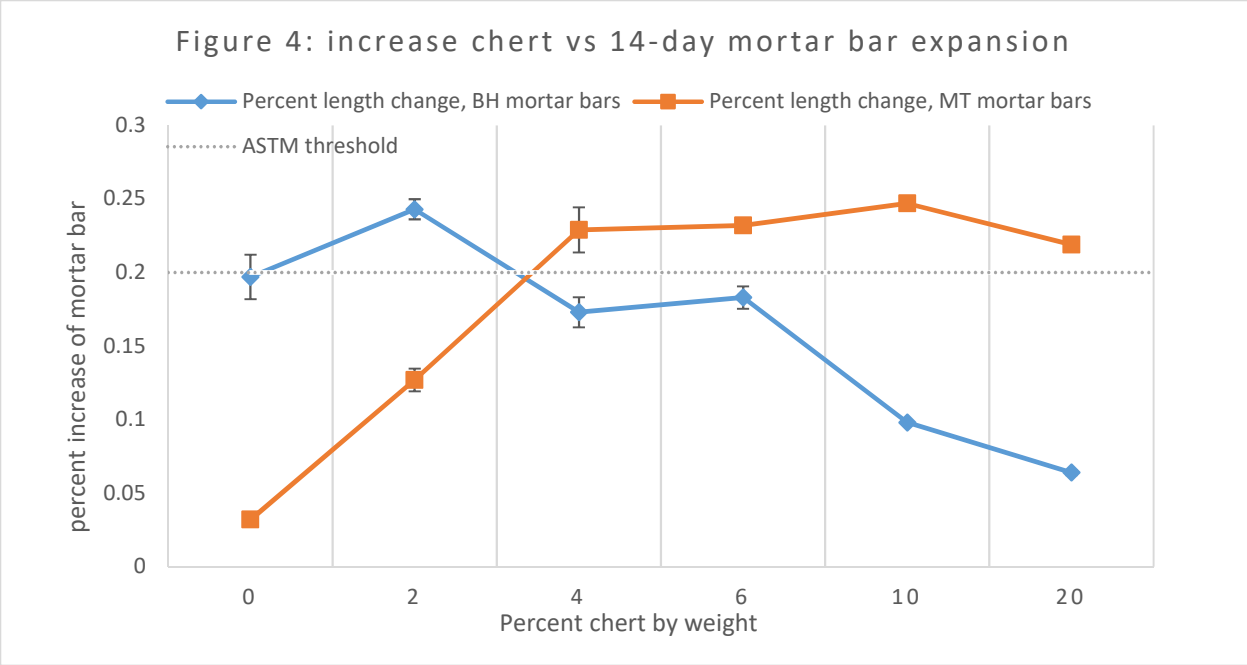

Figure 4. A comparison of BH and MT mortar bar expansion with increasing chert.

5.3 Alkali hydroxide concentration measurements

After the 14-day expansion trials, bars containing MT- aggregate were removed from solution and dried. The concentration of solution batches was measured via titration, and plotted to show the relationship between mortar specimen expansion and alkali consumption (Figure 5). Molarity concentration is converted to g/µm^3 and the difference from initial concentration of 4.00E-14 is used as the value for *rs* in Eq. 1 to solve for diffusivity *D* (presented in section 5.5 below). While precision of the titrations was not measured, it was estimated that visual observation of equivalence point is within 1.5ml, or +/- 0.013 M.

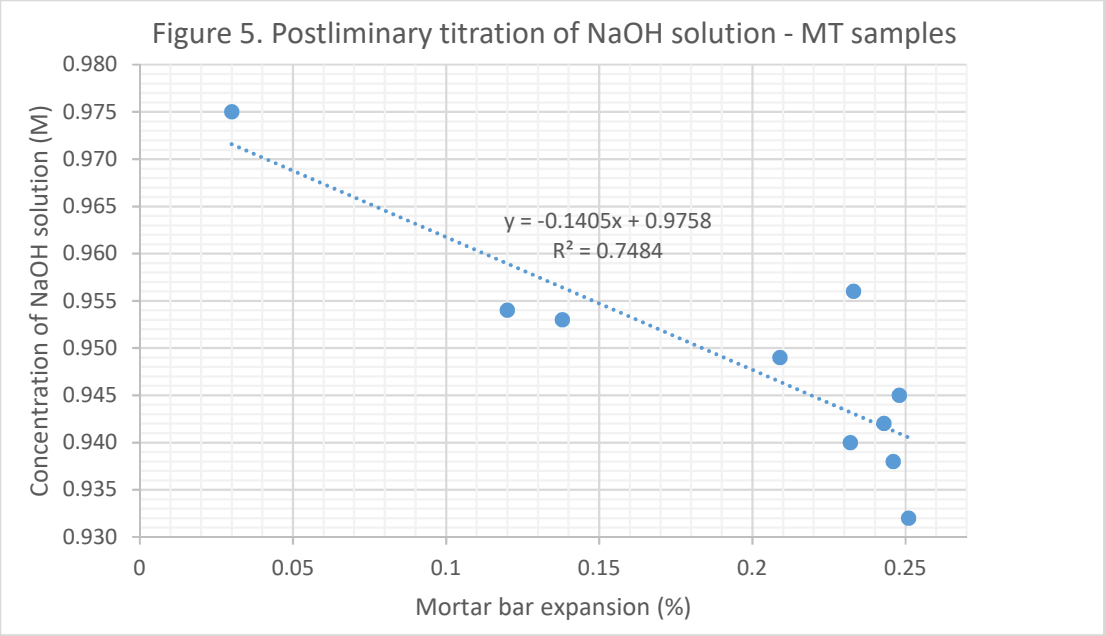

Figure 5. Titration results of 10 alkali solution samples taken after ASTM C1260 tests. Concentration of solutions from MT-0 through MT-10 trials were plotted against mortar bar expansion.

5.4 Observations under thin section

Chert was identified under plane and cross polarized light as angular to subangular grains consisting of microcrystalline quartz or silica fragments. Chert grains under thin section exhibit two general categories of degredation: micro-splaying and centripetal fracturing, or diffusive reaction rims. In comparison, between chert grains fractures were not consistent in scale, differing in frequency and width. Some grains exhibited both types of degredation, as diffusion developed along these fractures and penetrated past reaction rim depths and into further into grain interiors (Appendix B, Figures B-6 and B-7).

Three types of outliers were identified when performing the measurements. First, where thin sections were cut along the surface of chert grains, up to 0.8mm reaction rims were observed. These were considered as unavoidable products of thin section procedures, and appear to overestimate the actual dissolution penetration. Second, smaller chert grains less than 0.3 mm in diameter were observed to be completely enveloped with reaction rims and therefore underestimate dissolution penetration. And last, were large fractures in several grains that dissolved the inner portions of the grain simultaneous to diffusion.

From five petrographic slides, 25 individual chert grains were identified from BH-10 thin section samples. Where apparent, reaction rims were measured between the chert-cement contact surface and the unreacted inner chert grain. From this dataset, I obtained a range of reaction depths between 0.14mm and 0.5mm. The ranges of values were used for X in Eq. 1 to solve for diffusivity D. (presented in section 5.5 below). The average reaction depth from the 25 measurements was 0.27mm with a standard deviation of 0.10mm. Using the average value as an

example, the model predicted a non-linear association between penetration depth (µm) and alkali concentration (g/µm^3) with a given time of 14 days (Figure 6). Reaction rim depth measurements are provided in Appendix A, Table A-2.

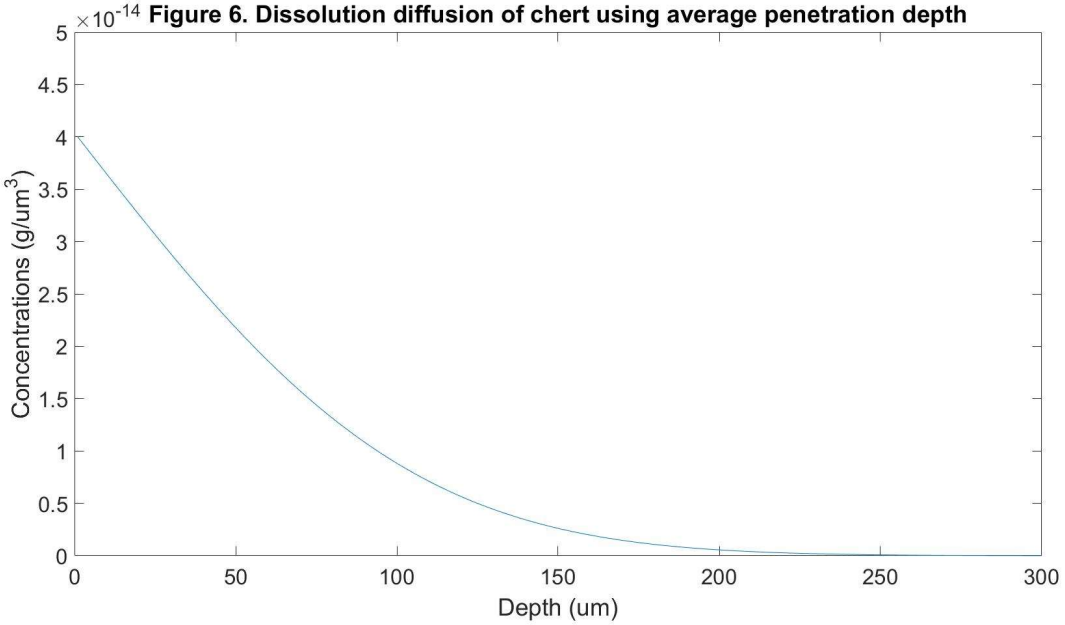

Figure 6. An example of diffusion model using the mean diffusivity of 2.7E-15 and the mean penetration depth at 0.27mm. This plot shows the concentration of alkali at increasing depth into a chert grain.

5.5 Diffusion modeling

Variables for Eq.1 were obtained from values directly observed in the experiment. *Cs* is a fixed value at 4.00E-14 g/µm^3 converted from alkali solution molarity. *Co* is some end depth concentration of 0 g/µm^3. Variable *Y* is some concentration along some distance of *X*. The time of 14 days is converted to seconds to yield 1.21E6 s, and *rs* is estimated using the loss of concentration of alkali in BH-10 samples, as indicated in section 5.3 above.

Solving variable *D* using input values (provided in Table 5) yields a diffusivity between 9.5E-16 µm^2/s to 8.0E-15 µm^2/s. Since *rs* is not significantly affected by the amount of reactive silica, the model predicts near constant diffusivity of chert for all aggregate samples. I explain in section 6.1 below that some pessimum effect acts on samples with higher proportions of chert. However, the dissolution of silica is seen as an independent process from pessimum, and is only affected by scarcities of available silica and alkali needed for reaction to occur. Pessimum was not observed to alter the diffusivity of reaction in chert grains.

Table 5. Input values for diffusivity model BH-10 aggregate	
Variable	**Input**
Y (alkali concentration at time t)	-
X (penetration distance at time t)	140 µm – 440 µm
Cs (surface concentration)	4.00E-14 g/µm^3
Co (concentration at x depth)	0
T (time)	1.21E6 s
rs (reactive silica consumption)	3.8E-17 g/µm^3
D (diffusivity)	Range: 9.5E-16µm^2/s – 8.0E-15µm^2/s Mean: 2.7E-15µm^2/s

6.0 Discussion

6.1 Pessimum Proportion

Bažant and Steffens (2000) suggested that swelling due to ASR is resisted by concrete, which develops internal pressures. It is this expansive pressure that is accumulated in the boundary region between aggregate grains and surrounding cement paste. Swelling pressure is limited by the amount of reactive aggregate available for ASR, and by the available calcium necessary for gel formation. This is the idea of pessimum proportion, where a certain proportion of some reactive aggregate causes the largest expansion, and that the expansion decreases when the content of the reactive aggregate increases or decreases from that proportion (Stanton, 1941). Based on the titration data presented in section 5.3, there is insubstantial consumption in NaOH(aq) during the mortar expansion tests. This confirms findings by Bleszynski and Thomas (1998) that alkali hydroxides are not the limiting component for inducing pessimum proportion effects.

This pessimum proportion was identified in BH and MT mortar bars containing 2% and 10% chert, respectively. The control aggregate used in BH mortar bars contained reactive aggregate with high expansive potential. In contrast, MT bars using only control aggregate were innocuous. MT bars therefore required more chert than BH to reach pessimum proportion.

Based on the observations in this project and previous studies on ASR gel, two theories are proposed to explain pessimum proportion:

1. Exceedance of optimum silica-alkali ratio

Given a period of time and concentration of hydroxides, ASR (and swelling pressure) may not always increase with increasing proportion of chert, and is maximized at the proportion at which ASR is most efficient. The limitation of swelling pressures appears to reflect both the diffusive efficiency of the aggregate and the rate of silica dissolution. As the proportion of reactive aggregate increases, a larger surface area allows for an increase in ASR gel production and assumed expansive pressure. Dent Glasser and Kataoka (1981) suggest an optimum silica to alkali ratio ($SiO_2/Na2O_e$) where the dissolution of silica in alkali solution is at the most efficient at a

given pH. If this ratio is then exceeded (by increasing amounts of reactive aggregate), there is a plateau in the quantity of silica in contact with solution, and therefore a stagnation in ASR gel formation. For this to occur, the dissolution reaction requires a low actual yield.

2. Limitation of $Ca(OH)_2$ and changes in gel composition

Gel formed from ASR is not a fixed composition, and varies with distance from aggregate reaction sites (Knudsen and Thaulow, 1975). The dissolution of silica primarily involves the attack by hydroxl on reactive aggregate. This dissolved silica reacts with $Ca(OH)_2$ to produce depolymerized C-S-H. In contrast to monovalent Na^+ or K^+, researchers have suggested that the higher valence of Ca^{2+} ions initiate cross linking of silicate ions (Gaboriaud et al., 1999). This catalytic ability of calcium is thought to be an integral part of C-S-H and A-S-H gel formations. If, however, the available $Ca(OH)_2$ is limited, the amount of calcium linked silicate polymers would be diluted by an increase in dissolved silica and smaller unlinked silicate polymers. This decrease in calcium/silica ratio may lead to the formation of lower viscosity gels, and thus decreased swelling pressures.

Similar effects of pessimum proportion were exhibited with portioned replacement of cement with fly ash. Fly ash, consisting of burnt pulverized coal, has very low alkali and calcium and is thus used as partial replacement of cement in concrete to reduce the effects of ASR expansion (Carrasquillo and Snow, 1987). The fly ash reduces the alkalinity of pore solution, reducing the calcium silica ratio of C-S-H gel (Shafaatian et al., 2013).

In contrast, Powers and Steinour (1955) distinguished non-expansive and expansive gels based on the amounts of calcium and alkalis in the reaction products. They implied that high calcium gels were introduced as non-swelling or “safe” gels. Prezzi (1997) showed that expansive gels is primarily due to double-layer forces between ions, and that thicknesses of those forces depend on the valence size of the ions. Therefore, low CaO/Na_2Oe contents would theoretically cause larger expansion in mortar samples. Since ASR gel is complex and has varying compositions, it is difficult to identify the component responsible for pessimum proportion. However, researchers agree that calcium plays an integral role in gel formation (Struble and Diamond, 1981a, 1981b, Thomas, 1998, 2001; Hou et al., 2004).

6.2 Aggregate composition

In my experiments, BH-mortar bars containing low or no chert (2% to 0% aggregate compostion) expanded the greatest amongst the BH aggregate/mortar tests. With little or no chert, it is therefore possible that both the cement and reactive silica within BH-aggregate contribute to this expansion. Within cement, the amount of comprised silica was previously found to be 20.1%. Using the same cement, mortar bars containing MT control sand showed minimal expansion. It is therefore suspected that expansion of the BH mortar bars was primarily due to the aggregate which contains approximately 28% volcanic lithics.

Andesite has been long documented to cause ASR (Holland and Cook, 1953; Kawamura et al., 1989; Wakizaka et al., 1989; Wakizaka, 2000). Using variations on mortar bar expansion tests, researchers have observed andesitic aggregate expansions of up to 0.5% (Kobayashi et al., 1989). Šťastná et al. (2013) conducted accelerated mortar bar tests using crushed volcanic aggregates from a variety of locatities across the Bohemian Massif, Czech Republic. Their results indicate that moderate to high ASR potential occurs in volcanic aggregates with increasing felsic constituents and silica rich phases.

The reactivity of andesite is due to the component of silica both within the groundmass and within phenocrysts. Shiraki and Kobayashi (1989) found the chemical composition of glass in five andesite samples to be greater than 70% silica. Generally, volcanic glass in andesite forms during an uncrystallized phase within imperfect growth of microcrystals in groundmass. Glass also exisits within phenocrysts, as partial melting of phenocyrsts can occur in contact with higher temperature magmas (Tsuchiyama and Takahashi, 1983). Cristoballite and tridymite may also exist in the groundmass and within vesicles of andesitic rock, as they form under the metastable ranges of high temperatures during the late stage of magma crystallization. The presence of silica, in the form of glass, cristoballite, and tridymite all contribute to the potential expansive properties of andesite.

6.3 Reaction rims and diffusion mechanism

The dense and dark reaction rims observed in the thin sections are similarly described by Ichikawa and Miura (2007) and are apparent in many chert grains from mortar bars subjected to ASTM C1260. However, under PLM, an uneven distribution of ASR within grains is notable. To examine this, one must envision ASR working at two scales: ~1µm in which fractures are prevalent at grain surfaces, and ~10^{-4}µm in which the size of alkali hydroxides allows a diffusive penetration into grains. Several ~1um fractures were observed under SEM (Figure 7) that may serve as alkali gateways, a source of accelerated transmission of alkali to inner grain structures. This further enhances the rate of silica depolymerization via diffusion. These fractures are not distributed evenly throughout the grain surface, thereby leading to inhomogeneous distribution of ASR. Fracturing may increase the overall rate of diffusion into the grains by allowing pore solution to interact within the interior of the grains, and may thus enhance the diffusion mechanism.

The diverse angular geometry of the grains also affects the distance of ASR penetration observed under thin section. It is common that aggregates are alluvial sourced sand and gravel, exhibiting a high degree of natural rounding. As grains become increasingly rounded, the geometric variation within a population of grains might be reduced. However, it is also a common industrial practice that aggregate is produced via mechanical crushing of rock, thereby generating of angular fragments. With angular grains, the variation of surface area to mass increases.

Consider chert or any microcrystalline silica that has been previously crushed. The crushing of such materials results in flake like spalls that exhibit a high three-dimensional surface area to mass ratio. The higher surface allows for a higher rate of ASR and results in either greater or

lesser expansive pressure depending on sample pessimum. This angularity and low sphericity influenced my results by increasing the surface area of chert, thereby increasing the amount of reactive silica in proximity to cement pores and higher dissolution rate.

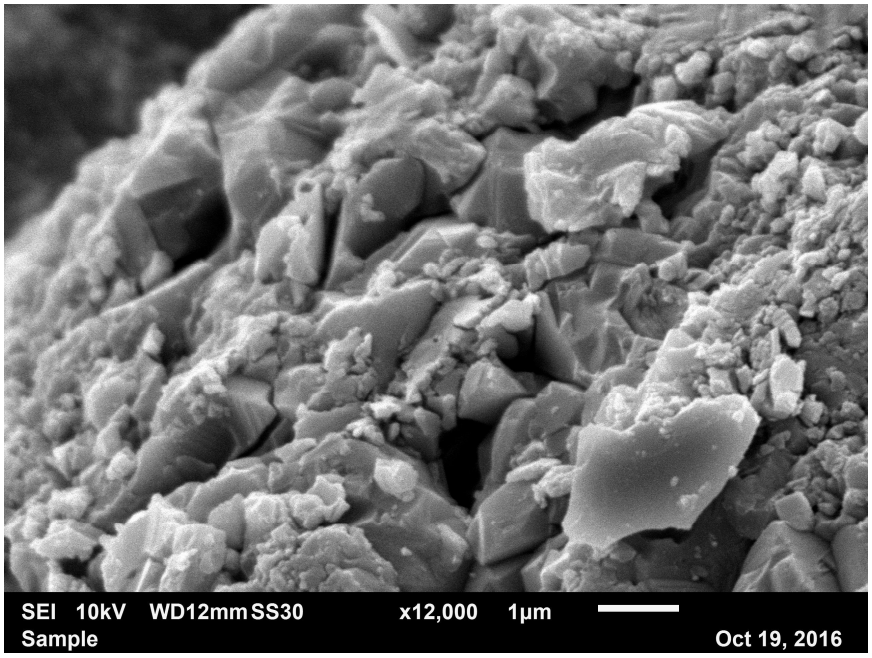

Figure 7. Observations of surface texture of chert under SEM are used to interpret interaction between silica and alkali. Cracks on the surface of chert, as seen in this image, may contribute to diffusion mechanism and increase diffusivity rates as it allows for penetration of alkalis into the grain.

6.4 Alkalinity reduction and dissolved silica content

Wakizaka et al. (1989) showed distinct relationships between the amount of dissolved silica, subsequent alkalinity reduction of alkali solution, and expansion in mortar bars. They suggest that these relationships are intrinsic to an aggregate's mineralogy, the properties of which define its thermodynamic metastability, amount of non-bridging oxygen, and crystallinity. My results of MT mortar bar titration tests also indicate that, below observed pessimum, there is a distinct relationship between mortar bar expansion and alkalinity reduction (Figure 5). Therefore, this suggests the ability to observe the expansion of concrete by chemical titration. Furthermore, assuming theoretical yield for depolymerization, the concentration of dissolved silica is calculated by the concentration loss in alkali solution. Silicate ions are precipitated by cations from solution, allowing up to four Na^+ ions from solution to bond to each available polymer. For example:

> Mortar bar specimen MT-C-4, containing 4 percent chert, expanded 0.246%. A titration test showed alkali reduction from 1.00M NaOH to 0.938M NaOH. Assuming one liter volume of solution, and excluding the alkali in cement, the amount of Na^+ that reacted to silicate ions was 0.0620 moles or ~3.73×10^{22} molecules. If we consider four Na^+ necessary

for bonding to each available silicate ion, the conservative estimate of dissolved silica is $9.33x10^{21}$ molecules, or 0.0155 moles, or ~1.43 grams.

By making assumptions about reaction yield, we can therefore quantify the mass of silicate released as a result of chert dissolution.

6.5 Diffusion modeling

The diffusivity values estimated by the simple diffusion model describes the rate of penetration of alkalis and hydroxides into the microscopic framework within the grains. The interaction between these ions and the silica framework results in systematic depolymerization. This depolymerization is the reactive intermediate that triggers cross linking of reactions by other available ions and forms alkali-silicates. The model does not account for the pH, pore fluid composition, or temperature under normal exposure of concrete structures. Also, the model does not account for the simultaneous reactions that generate the anisotropic chemo-physical properties of resultant gel. Rather it is utilized as a baseline estimation of available alkali-silicate ions necessary for C-S-H and A-S-H gel reactions.

The variability and degree of ASR in chert grains complicates the mathemetical abstraction involved in modeling the reaction rate. Although many have previously provided models in attempts to express ASR reaction rate (Sellier et al., 1995; Bablo et al., 2015; Ulm et al., 2000; Ichikawa and Miura, 2007), very little research has been done involing the effects of grain fractures acting as channels for accelerated ASR penetration, or the effects of angularity on reaction rate. Regardless, the simple diffusion model used here (eq. 1) approximates the depolymerization diffusivity of ASR in chert.

We see that reaction rims developed around andesitic grains, and that penetration is less than that of chert (Figure 8). This suggests a different ASR diffusion coefficient for these grains. With additional data, ASR rate could be predicted in grains, and may reveal information about andesite's susceptibility to depolymerize. The unique structures of different silica polymorphs or rocks may control the ASR diffusion rate. If we assume diffusion is the primary mechanism for reaction in silica, we can begin to understand the relationship between different microcrystalline frameworks and the rate of ASR.

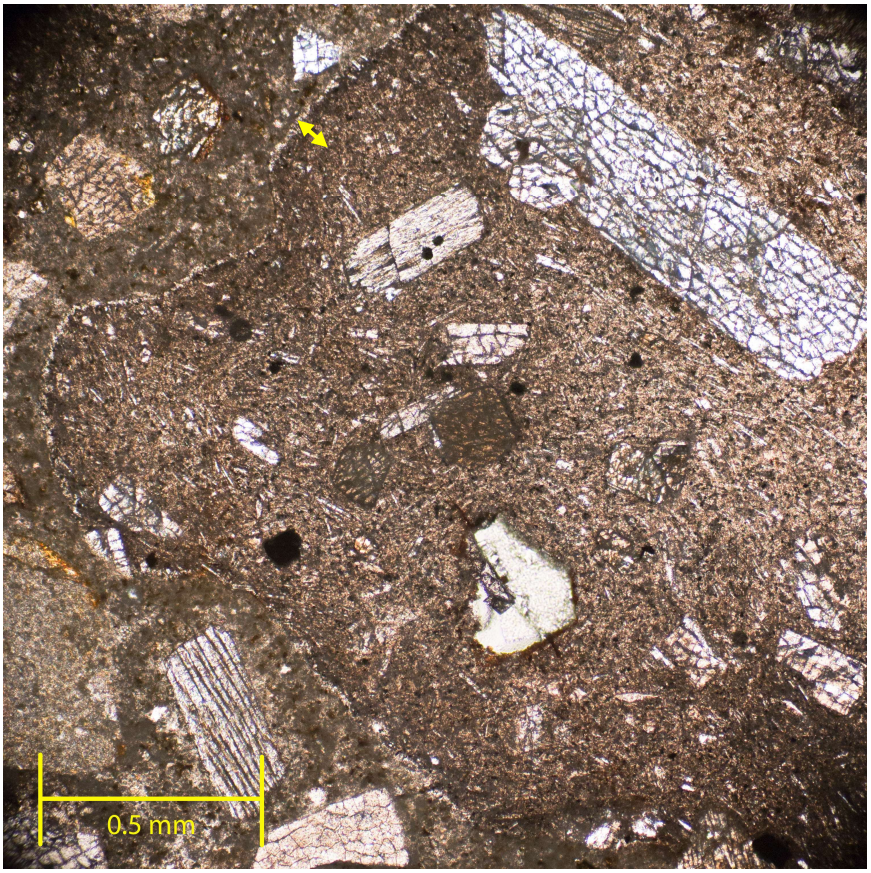

Figure 8. A grain of andesite from is observed under polarized light, filling most of the field of view of this image. Note the faint reaction rim that outlines the edges of the grain (yellow arrow).

6.6 Pessimum size effect

In addition to pessimum proportion, there exists a pessimum size effect where a certain effective grain size caused the largest concrete expansion, and that the expansion decreases when the grain sizes of reactive aggregate is increased or decreased from that effective size (Vivian, 1951; Diamond and Thaulow, 1974). I propose that the effective grain size is dependent on both the availability or concentration of alkali hydroxides and the efficiency in which ASR reacts within these grains. Consider reactive aggregate with some spherical grains of radius *r*, some sample volume V_1. Then consider the spherical grains of radius r/2 to represent grains half the size of the original aggregate. The number of grains required to meet the same aggregate volume batch in concrete would need to increase by eight.

$$V_1 = 4/3\pi r^3$$

If radius of V_2= r/2

$$V_2 = 4/3\pi(r/2)^3 = \pi r^3/6$$

$$\frac{V_2}{V_1} = 8$$

Now consider surface area of the grains with respect to decrease in grain radii. To meet volume batch requirements, grains half the size would increase the effective surface area by two.

$$SA_1 = 4\pi r^2$$

If radius of $SA_2 = r/2$

$$SA_2 = 4\pi(r/2)^2 = \pi r^2$$

$$\frac{V_2 SA_2}{V_1 SA_1} = 2$$

Based on my experiments, adding more reactive aggregate does not substantially affect dissolution rate. Reaction rate appears instead to be based on the ability of alkali hydroxides to diffusively penetrate the sample grains. This would mean: 1. diffusivity is constant regardless of grain size, and 2. finer-grained reactive silica may exert greater expansive pressure due to higher surface area, facilitating greater dissolution and silica gel production.

If the individual grains are efficiently diffusive, the ASR penetration distance in to the grain may exceed the diameter of the grain (Figure 9). In this scenario, the expansive pressure would then be limited, as the entirety of reactive aggregate has been consumed. Thus, the composition of the grains and the relationship between grain mineralogical structure and the diffusion rate becomes important.

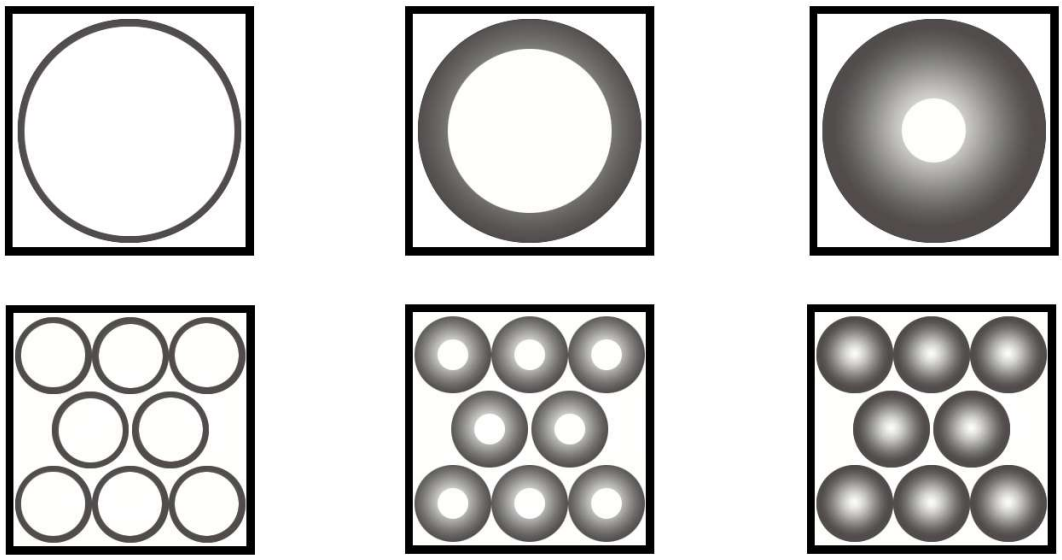

Figure 9. The figure shows a singular reactive aggregate grain, and eight smaller grains of equivalent mass. As time increases, alkalis penetrate diffusively into the grains at a rate regardless of grain radii. Gel forms within and along the surface of grains resulting in increasing swelling pressures. If the diffusion of alkalis penetrates fully into smaller grains, swelling pressure is capped. However, the larger grain will continue to exert increasing swelling pressure, as available reactive silica is not yet consumed.

Under PLM, the ranges of reaction rims in my experiments were observed to be consistent regardless of grain size. Chert grains less than ~0.3 mm in diameter were observed to be completely affected by dissolution from ASR. Since aggregate size was not altered in any of the samples, pessimum size effect could not be observed. It is assumed if the penetration distance of the reaction rim exceeded the radius of the grains, then the resultant swelling pressure from gel expansion would be limited. In contrast, if the reaction rim does not exceed the radius of the grains, then the gel would form unimpeded by available reactant supply.

6.7 Testing alternatives and recommendations

One motivation for this study was to address concerns regarding ASR-susceptible aggregate in western Washington. The local aggregate (BH) was indeed reactive, expanding nearly 0.2% percent even without added chert. In initial conversations with WSDOT, chert was named as the problematic component, but there is very little chert in the BH sand. It is evident from the experiments, that chert is not required for ASR-related expansion. A simple point count identified 28% volcanic lithic fragments (likely dominantly andesite), which has been identified in other studies to be susceptible to ASR. By adding just 4% chert in highly controlled aggregate (MT), the aggregate became reactive, expanding nearly 0.23%. This shows that chert and volcanic lithics have different susceptibilities of reaction in concrete.

One simple screening tool that could be employed by WSDOT is a compositional analysis of sands, avoiding any aggregate source that have more than a few percent volcanic fragments. Because the Cascade Volcanic arc is dominated by andesite, WSDOT could avoid aggregate sources with provenance in any of the Cascade volcanoes.

A second alternative to accelerated mortar bar expansion tests may be screening via titration, as described in section 6.4. A titration test can be run similarly to ASTM C1260, but requires only one measurement, at the end of the two-week trial. With a given cement type and composition, expansion is related to the amount of alkali consumed by ASR. Since different cements have different amount of equivalent alkali, a standardization of cement used in the titration tests is necessary to account for discrepancies in reproducing the results. While reaction byproducts are complex and heterogeneous, the total observed swelling pressure is simple and rather predictable based on reactant quantity. For this association to exist, it is also important that the volume of 1M alkali solution is predetermined. Furthermore, this alternative method is only effective prior to pessimum levels, as the chemistry of reaction products above pessimum change the expansive behavior of gels. Since I did not extensively experiment with titration past pessimum, I recommend further trails to be conducted to determine if additional alkali reduction to expansion relationships exist.

A possible supplement to the experiments performed on chert could be a parallel set of experiements on common volcanic components of reactive aggregate in western Washington State. Such experiements would generate the diffusion coeffcient for volcanic lithics, from which an estimate the silica available for ASR can be determined. In addition, a Brunauer-Emmett-Teller

(BET) surface area analyser may be useful in determining the surface area of certain reactive aggregates, as it provides a means to quantify the dissolution reaction efficiency. Further studies on slag substitutions and fly ash mitigation of reactive silica would benefit in the understanding of dissolution mechanisms.

7.0 Conclusion

A series of experiments were preformed to study the chemical behavior of silica metastability in concrete due to ASR. In running ASTM C1260 tests on mortar bars of known aggregate composition, ASR was observed at two different scales: as mortar bar expansion and as discolorations within the grains. Of the two types of aggregate sands used for mortar bars, comparatory measurements of samples BH-2 and MT-10 indicated the highest expansion at 0.24% and 0.25% respectively. In accounting for this difference in chert proportion between these sets of samples, it was found that volcanic lithics, mostly as andesite, contributed as reactive silica with chert in BH aggregates. Pessimum proportion was also observed when comparing BH-2 and MT-10 to their sample subsets containing higher amounts of chert.

Discoloration around chert grains was observed under thin section. From this observation, I proposed a diffusion type penetration of alkalis into chert grains. The rate of reactions as expressed by the diffusion coefficient for these grains may be thought of as a susceptibility factor related to lattice structure or internal damage of the silica mineral. It is possible that each type of silica polymorph or silica rock has its own ASR diffusion coefficient. Other factors such as alkali and silica concentration, temperature, and pH may also affect the reaction.

Chemical titration tests were also conducted to examine the loss of alkali from ASTM C1260 trials. The results from titration indicated a linear correlation between Na^+ concentration reduction and mortar bar expansion. The highest expanded mortar bar reduced the NaOH solution concentration from 1M to 0.93M. This indicates that available alkalis are present in excess, and are not the limiting reactant for pessimum proportion. Rather, pessimum proportion effects on mortar bars is attributed to the relative proportion of dissolved silica, Na^+, and Ca^{2+} that alter the viscous properties of alkali silica gels.

In addition to these experiments, a theoretical model was proposed to explain silica dissolution in reactive aggregate. This model was based Fick's law of diffusion. Observations of chert reaction rims in thin section showed consistencies to the diffusion mechanism. Mean reaction rim thickness was 0.27 mm for chert grains concrete of BH aggregate with 10% additional chert, after two weeks at immersed in NaOH solution at elevated temperature. From these observations, the range of diffusion coefficients of ASR for angular chert is between 9.5E-16$\mu m^2/s$ and 8.0E-15$\mu m^2/s$.

I conducted a point count of grains and found that 28% of BH sands contained volcanic lithics. A compositional survey of locally sourced aggregates was not performed. Therefore, the prevalence of volcanic lithics used as aggregate is unknown. A suite of experiments with various

proportions of volcanic grains, similar to those conducted here with chert, could identify “innocuous” levels of volcanic fragments in aggregate. Calculating dissolution rates could also be an important step in understanding the extent of ASR in these aggregates and predicting their behavior. These calculations allow the further quantification of silica concentration as dissolved reactants to form gels.

8.0 References

Alexander, G.B., Heston, W.M., and Iler, R.K., 1954, The solubility of amorphous silica in water: The Journal of Physical Chemistry, v. 58, p. 453–455.

Alexander, M.G., and Mindess, S., 2005, Aggregates in Concrete: London and New York, Taylor & Francis, p. 33.

ASTM, 2014, ASTM C1260-14 Standard Test Method for Potential Alkali Reactivity of Aggregates (Mortar-Bar Method): v. 04.02, p. 5.

ASTM, 2016, ASTM C150/C150M-16e1 Standard Specification for Portland Cement: ASTM International, v. 04.01, p. 10.

Bablo, F.A.N., Pianezzer, G.A., Gramani, L.M., Kaviski, E., and Teixeira, M.R., 2015, An Application to the Diffusion Equation in a Model for the Damage in Concrete due to Alkali-Silica Reaction: Applied Mathematical Sciences, v. 9, p. 4135–4147.

Baingam, L., Nawa, T., Iwatsuki, E., and Awamura, T., 2015, ASR formation of reactive chert in conducting model experiments at highly alkaline and temperature conditions: Construction and Building Materials, v. 95, p. 820–831, doi: 10.1016/j.conbuildmat.2015.07.179.

Barkov, A.Y., and Martin, R.F., 2016, Anomalous Cr-Rich Zones In Sector-Zoned Clinopyroxene Macrocrysts In Gabbro, Mont Royal, Montreal, Quebec, Canada: The Canadian Mineralogist, v. 53, p. 895–910.

Bektas, F., Turanli, L., Topal, T., and Goncuoglu, M.C., 2004, Alkali reactivity of mortars containing chert and incorporating moderate-calcium fly ash: Cement and Concrete Research, v. 34, p. 2209–2214.

Bleszynski, R.F., and Thomas, M.D.A., 1998, Microstructural studies of alkali-silica reaction in fly ash concrete immersed in alkaline solutions: Advanced Cement Based Materials, v. 7, p. 66–78.

Boggs, S., 1992, Petrology of sedimentary rocks, *in* New York, Macmillan, p. 206–216.

Boyer, L., Bensoussan, A., Durand, M., Grice, H., and Berard, J., 1985, Geology of Montreal, Province of Quebec, Canada: Environmental & Engineering Geoscience, v. xxii, p. 329–394.

Broekmans, M.A.T.M., 2004, Structural properties of quartz and their potential role for ASR: Materials Characterization, v. 53, p. 129–140.

Broekmans, M.A.T.M., 2002, The alkali-silica reaction : aspects of some Dutch concretes and Norwegian mylonites: 144 p.

Brown, E.H., 1987, Structural geology and accretionary history of the Northwest Cascades system, Washington and British Columbia: Geological Society of America Bulletin, v. 99, p. 201–214.

Cameron, V.J., 1989, The late quarternary geomorphic history of the Sumas Valley. M.S. Thesis:

Simon Fraser University, Burnaby, BC, Canada, 154 p.

Carman, P.C., 1940, Constitution of colloidal silica: Transactions of the Faraday Society, v. 36, p. 964–973.

Carrasquillo, R.L., and Snow, P.G., 1987, Effect of fly ash on alkali-aggregate reaction in concrete: Materials Journal, v. 84, p. 299–305.

Cheng, H.P., Barnett, R.N., and Landman, U., 2002, Structure, collective hydrogen transfer, and formation of Si(OH)4 in SiO2-(H2O)n clusters: Journal of Chemical Physics, v. 116, p. 9300–9304.

Daly, R.A., 1912, Geology of the North American Cordillera at the forty-ninth parallel: Canada Geological Survey Memoir, v. 38.

Davies, G., and Oberholster, R.E., 1986, The alkali-silica reaction product: a mineralogical and an electron microscopic study, *in* Proceedings of 8th International Conference on Cement Microscopy, Orlando, Florida, p. 303–326.

Dent Glasser, L.S., and Kataoka, N., 1981, The chemistry of “alkali-aggregate” reaction: Cement and Concrete Research, v. 11, p. 1–9.

Diamond, S., 2000, Chemistry and other characteristics of ASR gels, *in* Proceedings of the 11th International Conference on Alkali-Aggregate Reaction in Concrete, Quebec City, Canada, v. 31, p. 40.

Diamond, S., and Thaulow, N., 1974, A study of expansion due to alkali — silica reaction as conditioned by the grain size of the reactive aggregate: Cement and Concrete Research, v. 4, p. 591–607.

Dragovich, J.D., Norman, D.K., Haugerud, R.A., and Pringle, P.T., 1997, Geologic Map and Interpreted Geologic History of the Kendall and Deming 7.5-minute Quadrangles, Western Whatcom County, Washington: Washington Division of Geology and Earth Resources Open File Report 97-2, 39 p., 3 plates, scale 1:24,000, p. 45.

Dunn, T., and Sen, C., 1994, Mineral/matrix partition coefficients for orthopyroxene, plagioclase, and olivine in basaltic to andesitic systems: A combined analytical and experimental study: Geochimica et Cosmochimica Acta, v. 58, p. 717–733.

Easterbrook, D.J., 1962, Pleistocene geology of the northern part of the Puget Lowland: Washington [unpubl. Ph. D. dissert.]: Univ. of Washington, 161p.

Eby, G.N., 1984, Geochronology of the Monteregian Hills alkaline igneous province, Quebec: Geology, v. 12, p. 468.

Farny, J.A., and Kerkhoff, B., 2007, Diagnosis and Control of Alkali-Aggregate Reactions in Concrete: Portland Cement Association, p. 25.

Fernandes, I., 2005, Caracterização petrográfica, química e física de agregados graníticos em betões: Estudo de casos de obra. PhD dissertation, Universidade do Porto, Portugal: 334

pp.

Fernandes, I., 2009, Composition of alkali–silica reaction products at different locations within concrete structures: Materials Characterization, v. 60, p. 655–668.

Fernandes, I., Noronha, F., and Teles, M., 2007, Examination of the concrete from an old Portuguese dam: Texture and composition of alkali–silica gel: Materials Characterization, v. 58, p. 1160–1170.

Fernandes, I., Noronha, F., and Teles, M., 2004, Microscopic analysis of alkali–aggregate reaction products in a 50-year-old concrete: Materials Characterization, v. 53, p. 295–306.

Fick, A., 1855, Ueber Diffusion: Annalen der Physik und Chemie, v. 170, p. 59–86.

Gaboriaud, F., Nonat, A., Chaumont, D., and Craievich, A., 1999, Aggregation and gel formation in basic silico-calco-alkaline solutions studied: a SAXS, SANS, and ELS study: The Journal of Physical Chemistry B, v. 103, p. 5775–5781.

Glasser, F.P., 1992, Chemistry of the alkali-aggregate reaction, *in* The Alkali-Silica Reaction in Concrete, Blackie and Sont Ltd, p. 24.

Godfrey, E., 1908, Concrete: Pittsburg, Author, 118-126 p.

Gutteridge, W.A., 1985, The alkali-silica reaction in structural concrete, *in* Conference on Concrete in Construction, Stoneleigh, Warwickshire, UK, Stoneleigh.

Haha, M. Ben, 2006, Mechanical effects of alkali silica reaction in concrete studied by SEM-image analysis. Ph.D. dissertation: École Polytechnique Fédérale de Lausanne, 232 p.

Heaney, P.J., Banfield, J.F., Guthrie, G.D. (editor), and Mossman, B.T. (editor), 1993, Structure and chemistry of silica, metal oxides, and phosphates: Reviews in Mineralogy, v. 28, p. 185–223.

Helmuth, R.A., and Stark, D., 1992, Alkali silica reactivity mechanisms, *in* Skalny J (ed) Materials science of concrete III. American Ceramic Society, Westerville, p. 131–208.

Holland, W.Y., and Cook, R.H., 1953, Alkali Reactivity of Natural Aggregates in Western United States: Mining Engineering, v. 5, p. 991–997.

Hou, X., Struble, L.J., and Kirkpatrick, R.J., 2004, Formation of ASR gel and the roles of C-S-H and portlandite: Cement and Concrete Research, v. 34, p. 1683–1696.

Huang, P.M., Li, Y., and Sumner, M.E., 2012, Handbook of Soil Sciences: Properties and Processes: Boca Raton, CRC Press, 1442 p.

Ichikawa, T., 2009, Alkali–silica reaction, pessimum effects and pozzolanic effect: Cement and Concrete Research, v. 39, p. 716–726.

Ichikawa, T., and Miura, M., 2007, Modified model of alkali-silica reaction: Cement and Concrete Research, v. 37, p. 1291–1297.

James, C., and Hester, N., 1974, The distribution and physical properties of chert gravel in Pike County, Illinois: Illinois State Geological Survey, 35 p.

Johnson, S.Y., 1984, Stratigraphy, age, and paleogeography of the Eocene Chuckanut Formation, northwest Washington: Canadian Journal of Earth Sciences, v. 21, p. 92–106.

Johnson, S.Y., 1982, Stratigraphy, Sedimentology, and Tectonic Setting of the Eocene Cuckanut Formation, Northwest Washington. Ph.D. dissertation: University of Washington, 191 p.

Katawaki, K., Moriya, S., Wakisaka, Y., and Kato, O., 1989, Comparison of Results of the Chemical Method and Mortar Bar Expansion Test for Determining Aggregate Reactivity, *in* 8th International Conference on Alkali-Aggregate Reaction, Kyoto, p. 417–422.

Katayama, T., 2012, ASR gels and their crystalline phases in concrete—universal products in alkali–silica, alkali–silicate and alkali–carbonate reactions, *in* Proceedings of the 14th International Conference on Alkali Aggregate Reactions (ICAAR), Austin, Texas, p. 20–25.

Kawamura, M., 1998, Composition of ASR Gels and Expansion of Mortars: Materials Science of Concrete-Special Volume : The Sidney Diamond Symposium, p. 261–276.

Kawamura, M., and Iwahori, K., 2004, ASR gel composition and expansive pressure in mortars under restraint: Cement and Concrete Composites, v. 26, p. 47–56.

Kawamura, M., Koike, M., and Nakano, K., 1989, Release of alkalis from reactive andesite aggregates and fly ashes into pore soution in mortars, *in* Proceedings of the 8th International Conference on Alkali-Aggregate Reaction, Kyoto, p. 271–278.

Knudsen, T., and Thaulow, N., 1975, Quantitative microanalyses of alkali-silica gel in concrete: Cement and Concrete Research, v. 5, p. 443–454.

Kobayashi, S., Kawano, H., Morihama, K., and Ishii, Y., 1989, The Background of AAR Preventive Measures Adopted by the Japanese Ministry of Construction, *in* 8th International Conference on Alkali-Aggregate Reaction, Kyoto, p. 803–808.

Kovanen, D.J., and Easterbrook, D.J., 2001, Late Pleistocene, post-Vashon, alpine glaciation of the Nooksack drainage, North Cascades, Washington: Geological Society of America Bulletin, v. 113, p. 274–288.

LafargeHolcim, 2016, Cement mill test report #R-TI-16-07 (unpublished).:

Lapen, T.J., 2000, Geologic map of the Bellingham 1:100,000 quadrangle, Washington: Washington Division of Geology and Earth Resources open file report 5:, p. 1–15.

Leemann, A., Bernard, L., Alahrache, S., and Winnefeld, F., 2015, ASR prevention — Effect of aluminum and lithium ions on the reaction products: Cement and Concrete Research, v. 76, p. 192–201.

Locati, F., Marfil, S., Maiza, P., and Baldo, E., 2012, Characterization of ASR products in a 40-year-old highway. Province of Córdoba, Argentina: , p. 11.

McConnell, D., Mielenz, R.C., Holland, W.Y., and K.T., G., 1947, Cement-aggregate reaction in

concrete: Journal of the American Concrete Institute (Proceedings), v. 19, p. 93–128.

Mehta, P.K., and Monteiro, P.J.M., 2006, Concrete: microstructure, properties, and materials: 684 p.

Misch, P., 1966, Tectonic evolution of the northern Cascades of Washington State, *in* Tectonic evolution of the northern Cascades of Washington State: in Tectonic history and mineral deposits of the western Cordillera, in Canadian Institute of Mining and Metallurgy, Special Volume 8, p. 101–148.

Moundoungou, I., Bulteel, D., Garcia-Diaz, E., Thiéry, V., Dégrugilliers, P., and Hammerschlag, J.G., 2014, Reduction of ASR expansion in concretes based on reactive chert aggregates: Effect of alkali neutralisation capacity: Construction and Building Materials, v. 54, p. 147–162.

Mukhopadhyay, A., Ghanem, H., Shon, C.S., Zollinger, D., Gress, D., and Hooton, D., 2009, Mitigation of ASR in concrete-combined materials test procedure: Innovative Pavement Research Foundation, p. 161.

Owen, D.D., Leidy, J., Norwood, J.G., Parry, C.C., Pratten, H., Shumard, B.F., and Whittlesey, C., 1852, Report of a geological survey of Wisconsin, Iowa, and Minnesota: and incidentally of a portion of Nebraska Territory. Made under instructions from the United States Treasury department: Lippincott, Grambo & Company, 90-101 p.

Peterson, K., Gress, D., Van Dam, T., and Sutter, L., 2006, Crystallized alkali-silica gel in concrete from the late 1890s: Cement and Concrete Research, v. 36, p. 1523–1532.

Poole, A.B., 2005, Intoduction to alkali-aggregate reaction in concrete, *in* The Alkali-Silica Reaction in Concrete, New York, Van Nostrand Reinhold, p. 3–21.

Powers, T.C., and Steinour, H.H., 1955, An Interpretation of Some Published Researches on the Alkali-Aggregate Reaction Part 2-A Hypothesis Concerning Safe and Unsafe Reactions with Reactive Silica in Concrete, *in* Journal Proceedings, v. 51, p. 785–812.

Prest, V.K., and Hode-Keyser, J., 1975, Surficial geology, Montreal Island, Québec: Geological Survey of Canada, "A" series, scale 1:50,000, 1 sheet.

Prest, V.K., and Keyser, J.H., 1977, Geology and engineering characteristics of surficial deposits: Montreal Island and vicinity, Quebec: Ottawa, Energy, Mines and Resources Canada, 29 p.

Prezzi, M., Monteiro, P.J.M., and Sposito, G., 1997, The alkali-silica reaction, part I: Use of the double-layer theory to explain the behavior of reaction-product gels: ACI Materials Journal, v. 94, p. 10–17.

Rajabipour, F., Giannini, E., Dunant, C., Ideker, J. H., and Thomas, M. D., 2015. Alkali–silica reaction: current understanding of the reaction mechanisms and the knowledge gaps. Cement and Concrete Research, 76, p. 130-146.

Ramos, V.I.M., 2013, Characterization of the potential reactivity to alkalis of Portuguese aggregates for concrete. Ph.D. dissertation.: Ambiente e Ordenamento do Território, 516

p.

Šachlová, Š., Přikryl, R., and Pertold, Z., 2010, Alkali-silica reaction products: Comparison between samples from concrete structures and laboratory test specimens: Materials Characterization, v. 61, p. 1379–1393.

Sellier, A., Bournazel, J.P., and Mébarki, A., 1995, Une modélisation de la réaction alcalis-granulat intégrant une description des phénomènes aléatoires locaux: Materials and Structures, v. 28, p. 373–383.

Shafaatian, S.M.H., Akhavan, A., Maraghechi, H., and Rajabipour, F., 2013, How does fly ash mitigate alkali-silica reaction (ASR) in accelerated mortar bar test (ASTM C1567)? Cement and Concrete Composites, v. 37, p. 143–153.

Shiraki, R., and Kobayashi, K., 1989, Quality and quantity determinations of reactive substances in volcanic rocks, *in* 8th International Conference on Alkali-Aggregate Reaction, Kyoto, p. 567–572.

Shrimer, F.H., 2005, Progress in the Evaluation of Alkali-Aggregate Reaction in Concrete Construction in the Pacific Northwest, United States and Canada: U.S. Geological Survey Bulletin 2209-K, p. 11.

Sims, I., and Brown, B., 1998, Concrete Aggregates, *in* Hewlett, P.C. ed., Lea's Chemistry of Cement and Concrete, London, Arnold; Copublished in North, Central and South America by J. Wiley, p. 903–1011.

Smith, W.E., 1960, The siliceous constituents of chert: Geol. en Mijnb., v. 39, p. 1–8.

Smith, D.L., and Gilmour, E.H., 1979, The Mississippian and Pennsylvanian Systems (Carboniferous) Systems in the United States- Montana: USGS Professional Paper, v. 1110–X, p. 1–29.

St John, D.A., Poole, A.B., and Sims, I., 1998, Concrete petrography: a handbook of investigative techniques: Boca Raton, CRC Press, 593-594 p.

Stanton, T.E., 1941, Expansion of Concrete through Reaction between Cement and Aggregate ": Transactions of the American Society of Civil Engineers. Paper 2129, v. 107, p. 53–126.

Šťastná, A., Nekvasilová, Z., Přikryl, R., and Šachlová, Š., 2013, Microscopic examination of alkali-reactive volcanic rocks from the Bohemian Massif (Czech Republic), *in* The 3rd International conference on sustainable construction materials and technologies, Kyoto, 10 p.

Struble, and Diamond, S., 1981a, Swelling properties of synthetic alkali silica gels: Journal of the American ceramic society, v. 64, p. 652–655.

Struble, L., and Diamond, S., 1981b, Unstable swelling behaviour of alkali silica gels: Cement and concrete research, v. 11, p. 611–617.

Thaulow, N., Jakobsen, U.H., and Clark, B., 1996, Composition of alkali silica gel and ettringite in

concrete railroad ties: SEM-EDX and X-ray diffraction analyses: Cement and Concrete Research, v. 26, p. 309–318.

Thomas, M., 2001, The role of calcium hydroxide in alkali recycling in concrete: Materials Science of Concrete Special, p. 225–236.

Thomas, M.D.A., 1998, The role of calcium in alkali–silica reaction, *in* Materials Science of Concrete—The Sidney Diamond Symposium Westerville, OH: American Ceramic Society Bulletin, p. 325–337.

Tsuchiyama, A., and Takahashi, E., 1983, Melting kinetics of a plagioclase feldspar: Contributions to Mineralogy and Petrology, v. 84, p. 345–354.

Ulm, F.-J., Coussy, O., Kefei, L., and Larive, C., 2000, Thermo-Chemo-Mechanics of ASR Expansion in Concrete Structures: Journal of Engineering Mechanics, v. 126, p. 233–242.

Vivian, H.E., 1951, Studies in cement-aggregate reaction. XIX: the effect on mortar expansion of the particle size of the reactive component in the aggregate: Australian Journal of Basic and Applied Sciences, v. 2, p. 488–494.

Wakizaka, Y., 2000, Alkali – silica reactivity of Japanese rocks: v. 56, p. 211–221.

Wakizaka, Y., Moriya, S., Kawano, H., and Ichikawa, K., 1989, Mineralogical interpretations of dissolved silica and reduction in alkalinity of the chemical method, *in* Proc. 8th Int. Conf. on Alkali-Aggregate Reaction, p. 519–524.

Wenk, H.-R., Monteiro, P.J.M., and Shomglin, K., 2008, Relationship between aggregate microstructure and mortar expansion. A case study of deformed granitic rocks from the Santa Rosa mylonite zone: Journal of Materials Science, v. 43, p. 1278–1285.

Wieker, W., Hubert, C., Heidemann, D., and Ebert, R., 1998, Alkali–silica reaction—a problem of the insufficient fundamental knowledge of its chemical base, *in* Materials Science of Concrete (Sidney Diamond Symposium), The American Ceramic Society, Ohio, USA, p. 395–408.

Wieker, W., Hubert, C., Heidemann, D., and Ebert, R., 2000, Some experiences in chemical modelling of the alkali-silica reaction, *in* 11th International Conference on Alkali-aggregate Reactions, Quebec, p. 119–128.

WSDOT, 2016, Standard Specifications for Road, Bridge, and Municipal Construction M 41-10: http://www.wsdot.wa.gov/publications/manuals/fulltext/M41-10/2016Amended2016-01-04.pdf (accessed January, 2016).

Young, G.., 1958, Interaction of water vapor with silica surfaces: Journal of Colloid Science, v. 13, p. 67–85.

Appendix A – Tables

Appendix A – Tables

Table A-1 Mortar bar specimen, related chert content, and 14 day expansion		
Mortar Bar Specimen ID	**Chert Content in aggregate (%)**	**14 day expansion (%)**
BH-0-A	0	0.218
BH-0-B	0	0.192
BH-0-C	0	0.182
BH-2-A	2	0.226
BH-2-B	2	0.225
BH-2-C	2	0.240
BH-4-A	4	0.187
BH-4-B	4	0.164
BH-4-C	4	0.167
BH-6-A	6	0.172
BH-6-B	6	0.189
BH-6-C	6	0.187
BH-10-A	10	0.098
BH-10-B	10	0.097
BH-20-A	20	0.065
BH-20-B	20	0.062
BH-20-C	20	0.066
MT-0-A	0	0.037
MT-0-B	0	0.028
MT-0-C	0	0.030
MT-2-A	2	0.138
MT-2-B	2	0.124
MT-2-C	2	0.120
MT-4-A	4	0.209
MT-4-B	4	0.233
MT-4-C	4	0.246
MT-6-A	6	0.232
MT-6-B	6	0.232
MT-10-A	10	0.251
MT-10-B	10	0.248
MT-10-C	10	0.243
MT-20-A	20	0.217
MT-20-B	20	0.219
MT-20-C	20	0.220

Table A-2 Summary of reaction rim measurements			
Chert ID	**Diameter (mm)**	**Diffusion or fractures?**	**Reaction Rim Size (mm)**
1	2.50	Diffusion	0.38
2	0.92	Diffusion	0.18
3	0.84	Diffusion	0.18
4	1.15	Diffusion	0.44
5	0.82	Diffusion	0.5
6	0.92	Diffusion	0.17
7	2.90	Diffusion	0.44
8	2.10	Diffusion	0.38
9	1.70	Diffusion	0.3
10	1.80	Diffusion	0.36
11	1.00	Diffusion	0.26
12	1.80	Diffusion	0.2
13	2.20	Diffusion	0.3
14	1.40	Diffusion	0.44
15	0.94	Diffusion	0.18
16	0.60	Diffusion	0.24
17	1.04	Diffusion	0.18
18	0.42	Diffusion	0.14
19	0.60	Diffusion	0.2
20	1.34	Diffusion	0.22
21	0.58	Diffusion	0.24
22	0.94	Diffusion	0.16
23	0.46	Diffusion	0.2
24	0.52	Diffusion	0.26
25	1.20	Diffusion	0.2
26	0.35	Fractures	N/A
27	1.15	Fractures	N/A
28	0.82	Fractures	N/A
29	0.30	Fractures	N/A
30	0.49	Fractures	N/A
31	0.92	Fractures	N/A
32	1.26	Fractures	N/A
33	1.10	Fractures	N/A
34	0.74	Fractures	N/A
35	1.24	Fractures	N/A
36	0.42	Both	0.14
37	2.50	Both	0.38

Appendix B – Figures

Appendix B – Figures

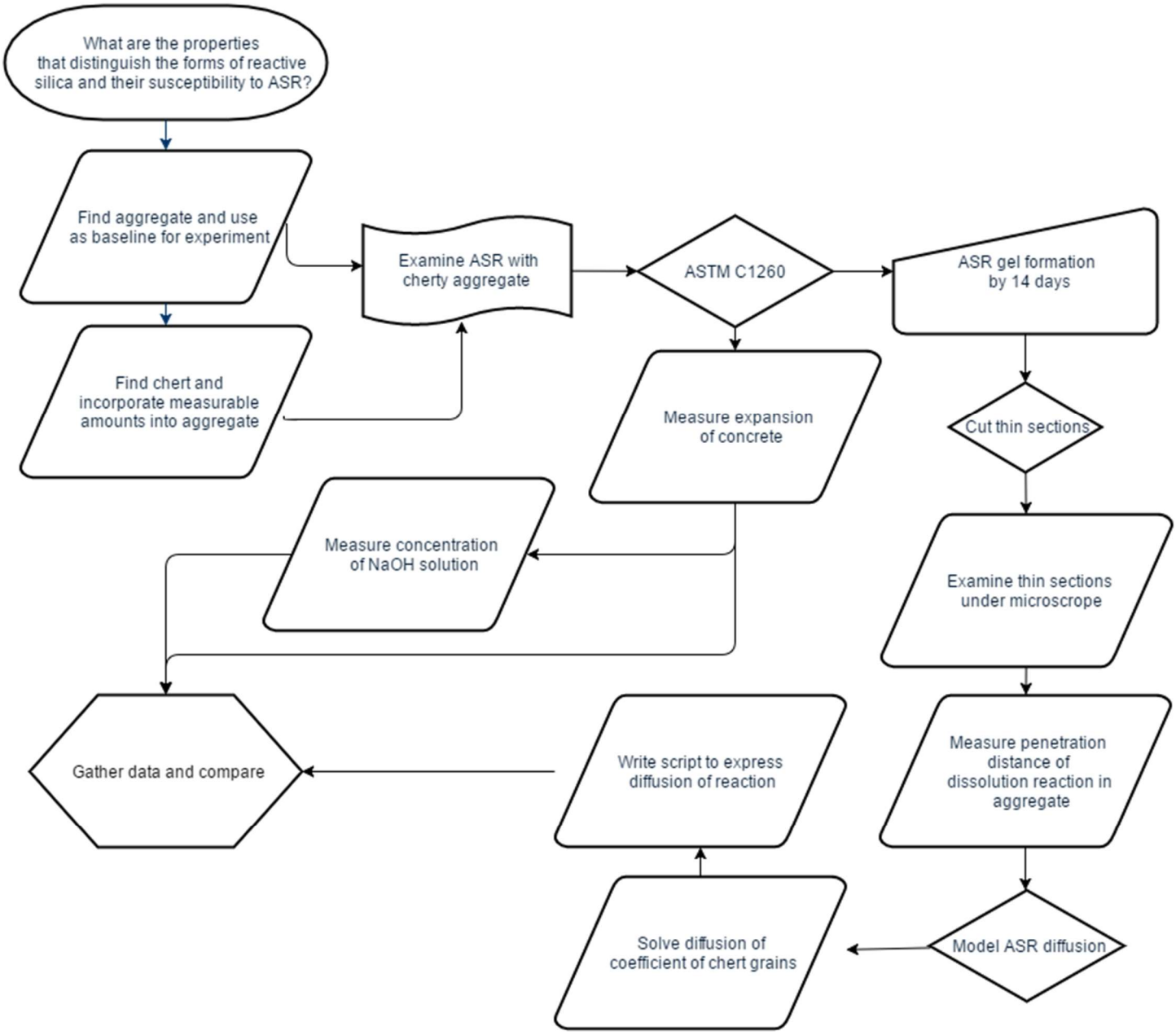

Figure B-1. Flow chart of project. A series of experiments were conducted to determine the connection of mineralogical characteristics of reactive silica effected by dissolution.

Figure B-2. Mortar molds were used to make the mortar bars. A triplicate subset of mortar bars for each ASTM C1260 trial was mixed into three of the four available molds. Prior to curing, the concrete was casted in the molds, then covered and stored in room temperature for a period of 24 hours.

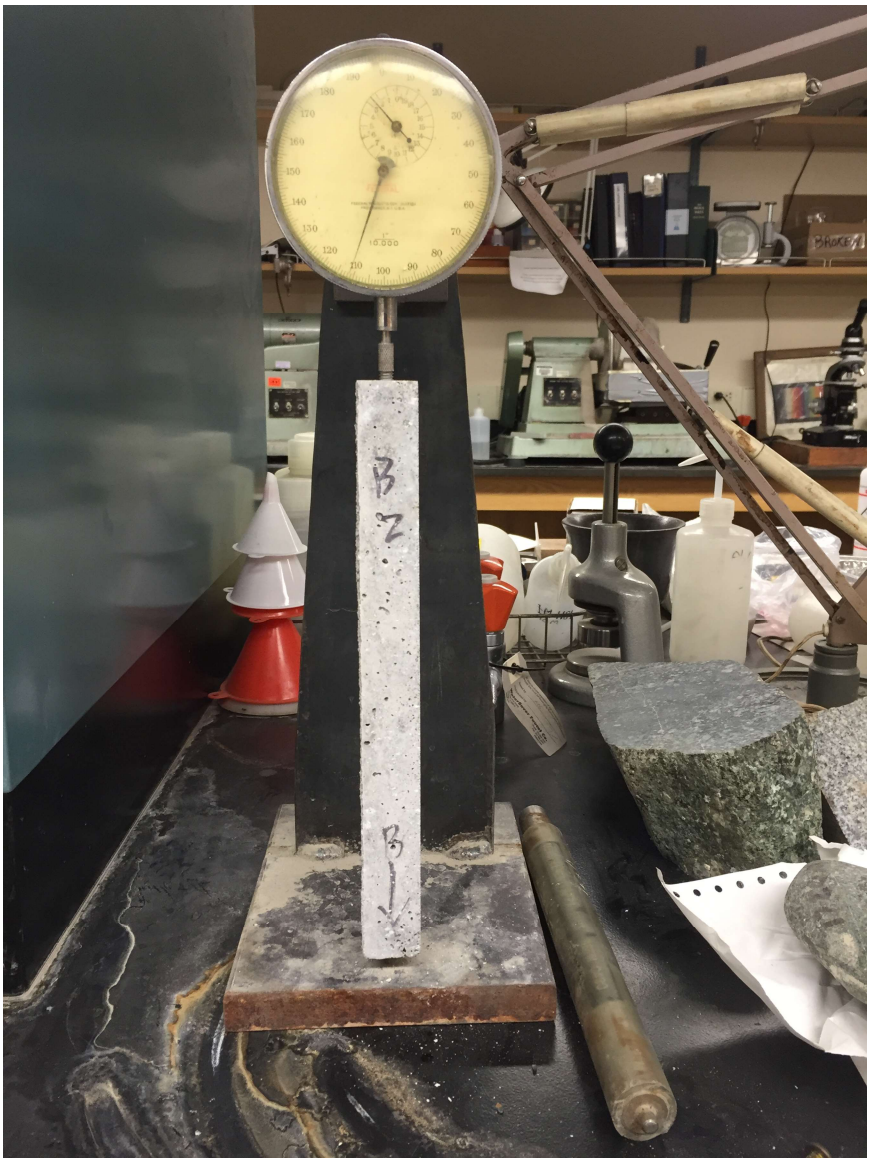

Figure B-3. The dial comparator used for the ASTM C1260 trials was accurate within 0.0001 inches. A reference bar (right of comparator), was used to zero the comparatory readings prior to each mortar bar measurement. The mortar bars were placed upright so that both gauge studs are on the comparator stage.

Photo B-4. Two Fisher Scientific ovens (Model 48) were used to maintain the temperature of specimens during the 14 day tests. High density polyethylene containers each contained 1L NaOH solution and one mortar bar specimen. These containers were placed horizontally, to ensure full submersion of solution.

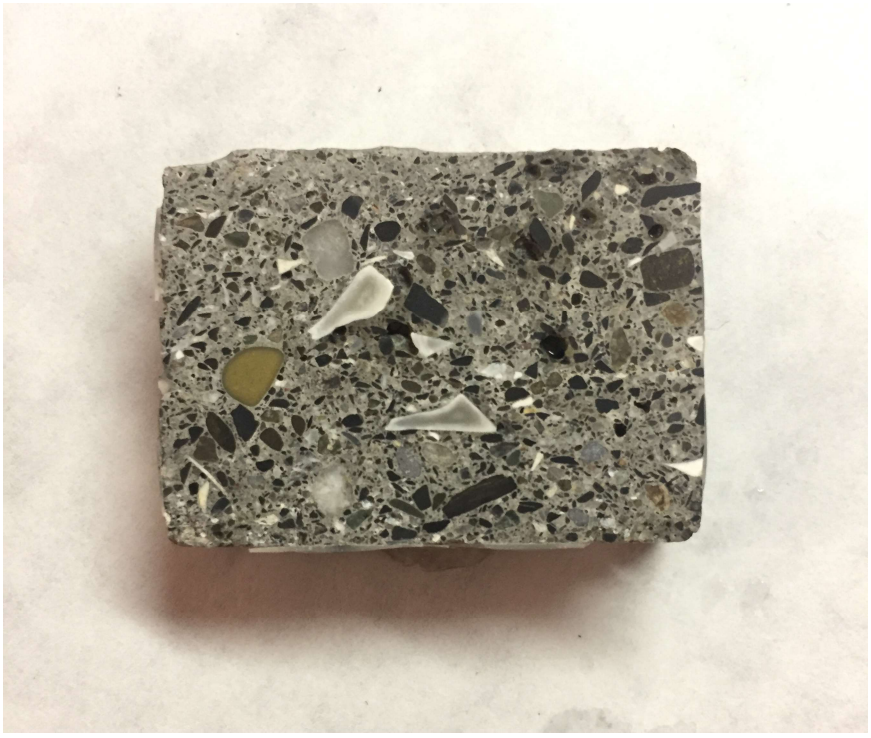

Figure B-5. Prior to thin section mounting, mortar bars were split and cut into blocks and polished. Chert grains can be identified due to their distinct angularity. Note the discoloration around the edges of the chert.

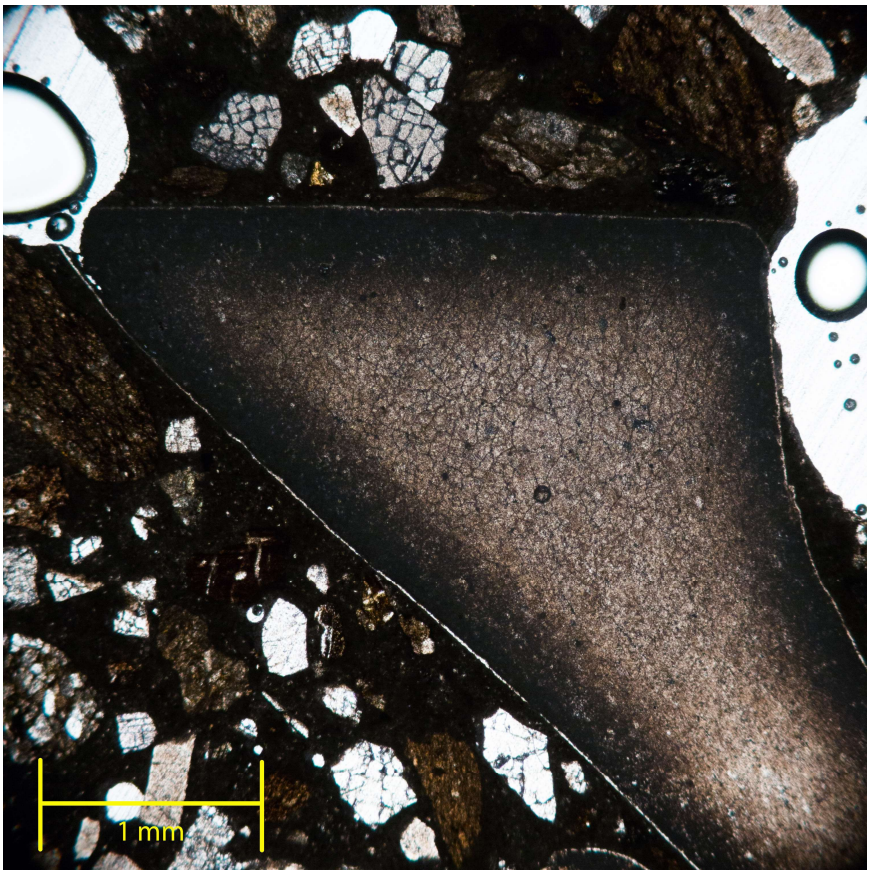

Figure B-6. In certain grains, micro fracturing was observed. In this example, diffusion is still apparent along the outer edges of the chert grain. However small fractures have developed internally.

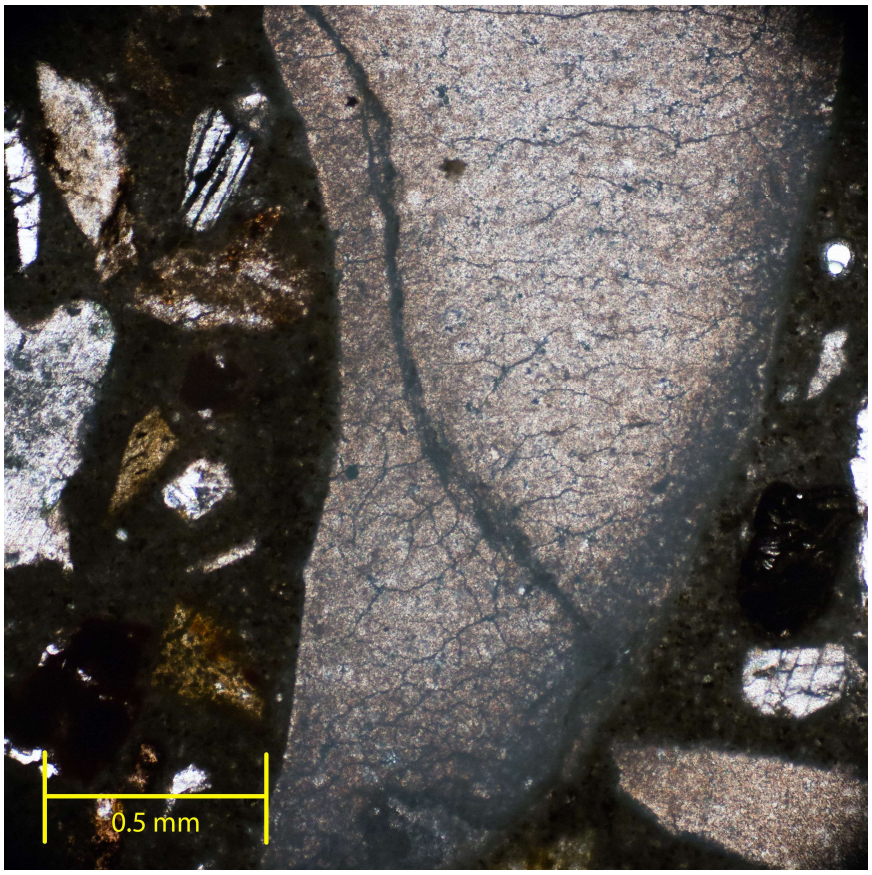

Figure B-7. Some grains was observed to have large fracture systems. In this example, dissolution reaction diffuses along a large fracture and through the grain.

Appendix C – Procedures

C-1 ASTM C1260 procedures

1.0 Purpose of application

This section describes the detection of potential for deleterious alkali-silica reaction of aggregate in mortar bars via modified ASTM C1260.

1.1 Equipment list

Table 1. List of Equipment	
Item Description	**Quantity**
1.5 Liter Naglene bottle	3
1”x1”x10” mortar bars	3
NaOH pellets	120 grams
Distilled water	3 liters
1 liter of tap water	3 liters
Fisher Scientific Model 48 Vacuum Oven	2
Length Comparator	1
Reference bar	1
1000 ml graduated cylinder	1
Electric balance	1
Nitrile gloves	2
Safety glasses	1

2.0 Method description

ASTM C1260 provides a means for detecting potential deleterious internal expansion resulting from ASR. The test is an accelerated mortar bar expansion test, detecting the severity of ASR expansion within 16 days from curing. By using a length comparator (sensitive to 0.0001 inches), length expansion of mortar bars can be documented. An expansion of 0.10% or less at 14 days as innocuous behavior. Expansions of more than 0.20% were indicative of potentially deleterious expansion. Between 0.10% and 0.20%, aggregates were considered to exhibit either innocuous or deleterious behavior in field performance

For the proposes of this project, the ASTM C1260 test has been modified to standardize the amount of NaOH solution per sample.

3.0 Procedure

3.1 Mixing NaOH solution

The experiment requires the mortar bars to be submerged in a 1M NaOH solution for a period of 14 days. One molar solution of NaOH was mixed using solid NaOH pellets and distilled water.

1. Measure out 750 ml of distilled water using the graduated cylinder.
2. Pour measured amount of water into an empty Nalgene bottle.
3. Measure out exactly 40 grams of NaOH.
4. Slowly stir in NaOH into bottle.
5. Measure out 250 ml of distilled water using the graduated cylinder.
6. Pour measured amount into Nalgene bottle with NaOH solution.
7. Stir until NaOH solids fully saturate.
8. Close the bottle.
9. Repeat twice for other two bars.

3.2 Initial storage and reading

Mortars are molded and left in the molding room covered in a moist cloth for a period of 24 hours (Appendix A). Then the bars are taken out of the molds and heat cured for a period of 24 hours.

1. Add approximately 1 liter of tap water into a Nalgene bottle and place one bar into the bottle. Repeat for other two bars.
2. Place bottles into oven and set to 80 degrees Celsius.
3. After a period of 24 hours, take the reference bar and mount it vertically on the comparator stage. While exerting a downward pressure on the top terminal, rotate the reference bar clockwise and record the lowest length as indicated on the dial.
4. Mount one bar onto the comparator state. When the bar is removed from the bottle, mount the bar on the comparator stage. Within 15 +/-5 seconds, exert a downward pressure on the top terminal, rotate the mortar bar and record the lowest length as indicated on the dial. Place the bar in a bottle filled with 1 liter of 1M NaOH solution
5. Record the time, bottle number, mortar bar sample ID, duration of experiment (number of elapsed days), reference bar reading, 15 second reading, and 5 minute reading.
6. . Close bottle tight and place back into oven.
7. Repeat for the remaining mortar bar samples.

3.3 Subsequent measurements

Subsequent comparator readings of the specimens are repeated every 24 hours for a period of 14 days.

1. After a period of 24 hours after previous readings, take the reference bar and mount it vertically on the comparator stage. While exerting a downward pressure on the top terminal, rotate the reference bar clockwise and record the lowest length as indicated on the dial.
2. Mount one bar onto the comparator state. When the bar is removed from the bottle, mount the bar on the comparator stage. Within 15 +/-5 seconds, exert a downward pressure on the top terminal, rotate the mortar bar and record the lowest length as indicated on the dial. Place the bar back into the sample bottle containing 1M NaOH solution.
3. Record the time, bottle number, mortar bar sample ID, duration of experiment (number of elapsed days), reference bar reading, 15 second reading, and 5 minute reading.
4. . Close bottle tight and place back into oven.
5. Repeat for the remaining mortar bar samples.

4.0 References

ASTM, 2016, ASTM C150/C150M-16e1 Standard Specification for Portland Cement: ASTM International, v. 04.01, p. 10.

C-2 Thin section procedures

1.0 Purpose and Application

This section describes the process for preparing concrete thin sections.

1.1 EQUIPMENT LIST

Table 1. List of Equipment	
Item Description	**Quantity**
Lapping wheel	1
Glass plate	2
120/220 grit abrasive	-
600 grit abrasive	-
1000 grit abrasive	-
Mechanical diamond cut-off saw	1
Cut off saw	1
Grinder	1
Petrographic slides 27x46mm	1
Vacuum pump	1
Devcon 2 ton clear epoxy (24 hour)	-

2.0 Method Description

Concrete thin sections are laboratory prepared 30 µm (0.03 mm) thick slice of concrete slabs that are attached to a glass slide with epoxy. They are used with a polarizing petrographic microscope to identify aggregate origin and concrete chemical reactions. The sections are left uncovered for purposes of additional chemical or SEM analysis.

3.0 Procedure

3.1 Sample preparation and initial cutting

Most commercial resin epoxies are hydrophobic, therefore the samples are washed with tap water and dried entirely prior to cutting. Mortar bar specimens are then rough cut using a

mechanical diamond cut-off saw. Bars are spliced in half and cut into approximately 25x50x12cm blocks.

3.2 Polishing concrete sample

After initial cutting, the blocks are polished using a three-tiered abrasive system to achieve a flat surface.

10. Turn on the lapping wheel and wet the surface with sufficient tap water until the grit is predominately saturated.
11. Pour a small amount (<1 oz) of 120/220 sized silicon carbide abrasive grit onto the lapping wheel.
12. With your hands, apply a downward pressure onto the concrete block sample so that the lapping wheel begins to flatten the bottom surface. Increase amount of grit material as needed.
13. Grid the surface for a period of ten minutes until surface appears to be free of thick points and depressions.
14. Rinse the concrete block using an ultrasonic cleaner.
15. Pour a small amount (<1 oz) of 600 sized silicon carbide abrasive grit, onto a glass plate and wet the surface with sufficient tap water until the grit is predominately saturated.
16. Lap the flat surface of the sample by applying a downward pressure onto the concrete block sample and the glass plate, for a period of ~30 minutes until the surface shows a polish sheen.
17. Rinse the concrete block using an ultrasonic cleaner.
18. Pour a small amount (<1 oz) of 600 sized silicon carbide abrasive grit, onto a second glass plate and wet the surface with sufficient tap water until the grit is predominately saturated.
19. Lap the flat surface of the sample by applying a downward pressure onto the concrete block sample and the glass plate, for a period of ~30 minutes until the surface shows a polish sheen.
20. Rinse the concrete block using an ultrasonic cleaner.

3.3 Ultra-violet epoxy impregnation

Since concrete has pore spaces, it is necessary to impregnate epoxy into the samples to prevent uneven mounting. A UV dye is used as an indicator for micro-cracks and pore holes.

1. Mix 4 drops of zyglo dye into 10 ml of low viscosity epoxy and hardener.
2. Within 10 minutes of mixing, lather dye/epoxy mix onto the concrete block surface.
3. Insert concrete sample into a vacuum oven and vacuum seal to ____ PSI for a period of 10 minutes.
4. Take samples out of the oven and let dry for a period of 24 hours.

5. Repeat section 3.2 until the epoxy is removed and a flat, polished surface is obtained again.

3.4 Preparation of glass slide

The glass slide must be flat to retain a constant thickness. Therefore, it is necessary to "frost" the slide, to remove thick spots and adjust the slide face with the grinding wheel's face.

1. Turn on grinder and release water valve to wet the grinder
2. Drag a corner of the glass slide onto the grinder and ground off the corner.
3. Place a second slide onto the slide holder of the cut-off saw.
4. Place the first slide onto the slide holder of the thin section grinder and turn on the vacuum pump (connected between the two instruments).
5. Turn the grinder control gauge to "0."
6. Turn on the grinder motor.
7. Move the slide back and forth so that the grinder is in contact with the entire slide surface.
8. Increase the gauge control by one dial or less.
9. Repeat step 7 until the slide is completely frosted as indicated by a matted texture.

3.5 Mounting

1. Heat the concrete sample by placing it on a hot plate and setting the heat dial to low (100 F). The mounted flat side should be upright.
2. Write the sample number in pencil on the frosted side of the petrographic slide.
3. Mix Devcon 2 ton clear epoxy with hardener using a small disposable mixing cup and wooden stick. Mix the epoxy and hardener at a ratio of 1:1
4. Once the epoxy is well-mixed, spread small amounts onto the top of the mounted side of the sample.
5. Carefully place the frosted side of the petrographic slide onto the epoxy covered surface.
6. Using the rubber eraser of a pencil, move the slide around the surface to expel bubbles. This will help in obtaining a parallel surface during grinding.
7. Allow the slide/sample to dry for a period of at least 24 hours.

3.6 Cutting

To accelerate the grinding process, a large portion of the block must be cut off.

1. Place the block mounted slide onto the cut-off saw slide holder.
2. Place a second slide onto the grinder slide holder and turn on the vacuum pump.
3. Release the water valve to wet the saw.
4. Using the control dial, adjust the distance of the slider holder approximately 2-3mm into the block.

5. Turn on saw motor.
6. Gently cut the block by moving the handle clockwise until the block is fully removed.
7. Turn off vacuum and saw motor.
8. Retrieve the block and slide.

3.7 Final grinding

1. Place a blank glass slide onto the cut off saw slide holder and turn on the vacuum pump.
2. Release the water valve to wet the grinder.
3. Turn the control dial counter clockwise until the slide can move freely past the grinder.
4. Turn on the grinding motor.
5. Move the slide back and forth so that the grinder is in contact with the entire slide surface.
6. Increase the gauge control by one dial or less.
7. Repeat step 6 until the thin section is approximately 0.30 μm thick.

4.0 References

Hirsch, D., 2012, How to make a thin section, Dave's methods at WWU Geology: https://davehirsch.com/other/thinsections/ (accessed September 2016)

C-3 Chemical titration procedures

1.0 Purpose of application

This section describes the titration of NaOH solution using a standard acetic acid solution. The object of this procedure is to determine the molarity of NaOH solution.

1.1 Equipment list

Table 1. List of Equipment	
Item Description	**Quantity**
NaOH solution (unknown concentration)	500ml
Acetic acid (6% v/v)	100ml
Phenolphthalein indicator (small bottle)	8 drops
300 ml Erlenmeyer flask	1
100 ml graduated cylinder	1
100 ml glass burette	1
Burette stand and clamps	1
500 ml right angle bent tip plastic storage squeeze bottle	1
Small plastic or glass funnel	2
Plastic chemical waste container	1
Nitrile gloves	2
Safety glasses	1

2.0 Method description

The equivalence point of a chemical reaction is the chemically equivalent quantity between an acid and base mixture. Because the equivalent point is the ratio of an acid to base as expressed by its stoichiometry, the concentration of an aqueous solution can be determined using a known concentration of reactant. Titrations are ideally used between a weak acid-strong base, or weak base-strong acid as they provide larger buffer indications for equilibrium. Since the pH of the reaction at the equivalence point is ~8.72, a phenolphthalein indicator is used as the halochromic chemical compound.

For this experiment, a 6% (v/v) acetic acid (CH_3COOH) solution is used as the standard base. This is first converted to molarity as follows:

v/v to ml:

$$6\% \left(\frac{v}{v}\right) = (0.06)(1000ml) = (60ml)$$

mass of acetic acid:

$$\rho_{\text{acetic}} * v_{\text{acetic}} = \left(\frac{1.05g}{ml}\right)(60ml) = 63g$$

molarity:

$$Molarity(1.00L) = \frac{\text{mass per liter}}{\text{molar mass}} = \frac{63g}{(60.0516g/\text{mol})}$$

$$Molarity = 1.0491M$$

The number of moles of CH_3COOH solution and NaOH solution are equal at equivalence, therefore the concentration of NaOH can be obtained with a known volume:

$$moles_{\text{CH3COOH}} = moles_{\text{NaOH}}$$

$$(M_{\text{CH3COOH}})(V_{\text{CH3COOH}}) = (M_{\text{NaOH}})(V_{\text{NaOH}})$$

3.0 Procedure

3.1 Titration of NaOH

1. Set up the burette by placing it on the stand using clamps. The burette should be vertical and approximately 15 cm from the base of the stand.
2. Carefully measure out precisely 100 ml of acetic acid using the graduated cylinder.
3. Pour measured amount of acetic acid into an empty Erlenmeyer flask.
4. Add 8 drops of phenolphthalein indicator into the flask.
5. Place flask onto the base of burette stand directly under the burette.
6. Twist the burette knob to close position
7. Carefully add 100 ml of NaOH (aq) into the burette using the plastic squeeze bottle.
8. Begin the titration by slowly adding NaOH (aq) from the burette to the acetic acid in the Erlenmeyer flask. Swirl the flask as you add the base in order to efficiently mix the chemicals.
9. If the entire 100 ml of NaOH (aq) has been mixed into the flask with not change in color, add an additional 20ml in the burette and repeat step 8.
10. As the equivalence point is approached, the pink color will become more pervasive and will take longer to disappear. When this occurs, start to add the NaOH (aq) drop by drop. Eventually the addition of just one drop of NaOH (aq) will turn the solution in the flask a

light pink color that does not disappear when swirled. This indicates that the equivalence point has been reached. If the pink color becomes vivid (instead of light and dilute), the equivalence is exceeded and the titration process will need to be restarted (back to step 1).

11. Measure this volume of NaOH (aq) precisely, recording the amount of volume of NaOH (aq) required for equilibrium.

3.2 Calculation

1. Calculate the molarity of NaOH (aq) from the moles of CH_3COOH and the volume of the NaOH (aq) sample used:

$$(M_{\mathrm{CH3COOH}})(V_{\mathrm{CH3COOH}}) = (M_{\mathrm{NaOH}})(V_{\mathrm{NaOH}})$$
$$(1.0491M)(100ml) = (M_{\mathrm{NaOH}})(V_{\mathrm{NaOH}})$$
$$M_{\mathrm{NaOH}} = 104.91moles/V_{\mathrm{NaOH}}$$

4.0 References

Santa Monica College, Titration of Vinegar:
https://www.smc.edu/AcademicPrograms/PhysicalSciences/Documents/Chemistry_10_Experiments/Ch10_Titration.pdf (accessed October 2016).

UC Davis, 2016, Acid-Base Titrations:
http://chem.libretexts.org/Textbook_Maps/Analytical_Chemistry_Textbook_Maps/Map%3A_Analytical_Chemistry_2.0_(Harvey)/09_Titrimetric_Methods/9.2%3A_Acid%E2%80%93Base_Titrations (accessed October, 2016).

Appendix D – Supplemental Data

Appendix D – Supplemental Data

```
close all; clear all; clc;

t=input('Enter Time in seconds: ');
D=input('Enter Diffusion Coefficient: ');
Cs=4E-14
Co=0
i=1;
y=(1:1:3000)
rs=3.8E-17

for x=(0:1E-6:3000E-6)
    if x <=3000E-6
        rs=0;
    else
        rs=0;
end
y(i)=((((Co-Cs)*(erf((x)/(2*(D*t)^(0.5)))))+Cs)-rs);
i=i+1;
end

plot(y);
xlim([0,250]);
ylim([0,5E-14]);
title('ASR Diffusion');
xlabel('Depth (um)');
ylabel('Concentrations (g/um^3)');
```

Figure D-1. Matlab script for diffusion model of Eq. 1. Note parameters *rs* and *Cs* as 3.8E-17 g/um3 and 4E-14E g/um3 respectively. This is based on concentration of solution from experiments.

Table D-1 ASTM C1260 daily length change of BH mortar bars*																	
Days	BH-0-A	BH-0-B	BH-0-C	BH-2-A	BH-2-B	BH-2-C	BH-4-A	BH-4-B	BH-4-C	BH-6-A	BH-6-B	BH-6-C	BH-10-A	BH-10-B	BH-20-A	BH-20-B	BH-20-C
0	0	0	0	0	0	0	0	0	0	0	0	0	0	0	0	0	0
1	24	0	2	5.5	5	-3	7	1	2	-9	-2	6	12	7	5	-6	6
2	21	8	8	8.5	16	9	9	8	3	-4	2	11	15	12	10	9	11
3	33	16	17	20	11.5	17	15	15	16	3	15	20	31	25	18	29	11
4	34	23	24	28	34	30	34	23	33	7	27	26	39	37	22	22	19
5	55	38	34	43	50	49	53	40	34	24	37	38	44	43	26	24	26
6	72	55	61	58	67	72	64	54	54	49	56	60	52	52	31	40	33
7	95	76	83	89	100	94	94	61	71	65	76	74	64	60	30	37	36
8	122	106	93	103	123	122	117	85	86	75	91	91	67	62	36	41	33
9	146	128	111	129	136	145	126	103	110	96	114	109	74	66	42	47	45
10	168	143	131	155	157	154	137	120	121	112	130	125	76	75	54	49	46
11	177	159	147	170	173	193	150	128	134	129	144	144	86	81	50	59	51
12	197	173	167	195	190	213	170	141	147	146	160	157	90	86	57	65	53
13	211	186	175	215	210	219	173	149	152	162	182	173	97	95	62	69	59
14	218	192	182	226	225	240	187	164	167	172	189	187	98	97	65	62	66
*Data is shown as 1/10000 inches.																	

Table D-2 ASTM C1260 daily length change of MT mortar bars*																	
Days	MT-0-A	MT-0-B	MT-0-C	MT-2-A	MT-2-B	MT-2-C	MT-4-A	MT-4-B	MT-4-C	MT-6-A	MT-6-B	MT-10-A	MT-10-B	MT-10-C	MT-20-A	MT-20-B	MT-20-C
0	0	0	0	0	0	0	0	0	0	0	0	0	0	0	0	0	0
1	-2	0	3	7	-4	-5	5	9	5	0	-4	6	3	-2	5	4	10
2	-1	0	-1	4	-1	6	5	9	10	5	3	13	9	6	16	17	18
3	3	0	4	4	4	4	14	25	14	18	19	28	31	23	33	32	27
4	2	0	7	16	11	18	26	55	44	37	40	62	59	39	49	40	42
5	-1	9	8	25	27	22	59	64	71	55	75	87	75	73	74	57	64
6	7	7	6	44	34	40	73	98	96	85	106	104	106	102	92	82	84
7	9	6	8	64	57	45	119	124	132	111	128	132	128	119	107	104	99
8	12	9	12	64	70	58	144	135	157	134	153	157	152	155	129	123	126
9	14	12	15	86	74	73	146	175	175	166	174	173	171	161	141	142	138
10	19	15	18	97	87	81	168	190	201	182	179	193	192	182	159	163	160
11	23	19	24	105	100	86	180	198	213	191	194	209	208	202	176	176	174
12	25	19	27	116	101	109	188	204	226	204	208	225	219	214	190	192	183
13	27	20	29	125	114	107	202	219	241	222	223	235	236	226	200	207	203
14	37	28	30	138	124	120	209	233	246	232	232	251	248	243	217	219	220
*Data is shown as 1/10000 inches.																	